2014

Examining Optimal Form of Two Scale Approximation (TSA) for Calculating Snl Source Term

Dorukhan Ardag
University of North Florida, dorukhan.ardag@gmail.com

EXAMINING OPTIMAL FORM OF TWO SCALE APPROXIMATION (TSA) FOR CALCULATING S_{NL} SOURCE TERM

by

Dorukhan Ardağ

A thesis submitted to the School of Engineering in conformity with the requirements for the degree of

Master of Science in Civil Engineering

UNIVERSITY OF NORTH FLORIDA

School of Engineering

April 2014

The thesis “Examining optimal form of Two Scale Approximation (TSA) for calculating S_{nl} source term" submitted by Dorukhan Ardag in partial fulfillment of the requirements for the degree of Master of Science in Civil Engineering has been approved by

The thesis committee: Date:

_____ _____
Dr. Donald T. Resio

_____ _____
Dr. William Dally, PE

_____ _____
Dr. Beyza C. Aslan

Accepted for the School of Engineering:

_____ _____
Dr. Murat Tiryakioğlu, CQE
Director of the School of Engineering

Accepted for the College of Computing, Engineering, and Construction:

_____ _____
Dr. Mark Tumeo, PE
Dean of the College of Computing, Engineering, and Construction

Accepted for the University:

_____ _____
Dr. Len Roberson
Dean of the Graduate School

ACKNOWLEDGEMENTS

First of all, I am extremely grateful to my committee chair and thesis advisor Dr. Resio, without his support, guidance and patience this thesis work wouldn’t be achievable. He introduced me to the topic and I benefitted a lot from his past experience on it, not to mention his superior knowledge on wind waves. In addition, I would like to thank, Dr. Dally and Dr. Aslan for agreeing to be on my master's thesis committee and spending time on giving countenance to my thesis work.

Also, I would like to thank Dr. Murat Tiryakioğlu for helping me greatly throughout the rough process of me arriving USA and being a part of the UNF Coastal Engineering Department. Along with that I am very grateful to my family, specially my mother and my brother, they`ve been always there for me with their personal support and encouragement even though there were thousands of miles between us.

TABLE OF CONTENTS

Chapter 1: INTRODUCTION 1

Chapter 2: METHODOLOGY 8

2.1. ENERGY TRANSFER BETWEEN WAVES AND THE FULL BOLTZMANN INTEGRAL 8

2.2. THE TWO SCALE APPROXIMATION AND THE DISCRETE INTERACTION APPROXIMATION 12

2.2.1. The DIA 12

2.2.2. The TSA 20

2.2.3. Benchmarking the Calculation Speeds of the TSA and the DIA 21

2.2.4. Performance Benchmarking between the TSA and the DIA 25

Chapter 3: MODIFICATIONS 29

3.1. PROGRAMS USED 29

3.1.1. The Specgen Program 30

3.1.2. The TSA 31

3.2. MODIFICATIONS 35

3.2.1. Changing the Domain & Resolution of the Local Scale 36

3.3. ADDITIONAL TESTS TO VERIFY MODIFICATIONS 44

3.3.1. Case 2: 25^{th} Ring – Apert = 4 44

3.3.2. Case 3: 21^{st} Ring – Apert = 4 50

3.4. RELAXATION OF THE INPUT SPECTRA 55

3.5. THE EFFECT OF MODIFICATIONS ON THE SPEED 56

Chapter 4: DISCUSSION 58

Chapter 5: CONCLUSIONS AND RECOMMENDATIONS 61

REFERENCES 64

FIGURES

Figure 1–1: New Spectra used in the Modified TSA. 5
Figure 2–1: The pumped transfer Tp (k_1, k_3) for k_1 (0.8, 0.8) (Webb, 1978) 11
Figure 2–2: Figure-8 Representation on Wave Number Space. 14
Figure 2–3: The DIA vs. The FBI for relative peakedness of 2.04 15
Figure 2–4: The DIA vs. The FBI for relative peakedness of 0.62 16
Figure 2–5: The DIA vs. The FBI for the relative peakedness of 4.32 17
Figure 2–6: 2D Comparison for Relative Peakedness of 2.04 18
Figure 2–7: 2D Comparison for Relative Peakedness of 0.62 18
Figure 2–8: 2D Comparison for Relative Peakedness of 4.32 19
Figure 2–9: Figure-8 Shape for Energy Transfer Integral 22
Figure 2–10: An individual grid cell for the DIA. 23
Figure 2–11: Comparisons of 1D nonlinear transfer (m2 Hz-1 s-1) for FBI, TSA, and DIA using Currituck Sound data for different locations called a, b, c and d respectively. (Resio & Perrie, 2009) 27
Figure 2–12: The 2D results (m^2 Hz^{-1} s^{-1}) using Currituck spectra for the FBI, the TSA, and the DIA for two different cases called “a” and “b”. (Resio & Perrie, 2009) 28
Figure 3–1: Specification of Integration Grid. Radius represents wave number or frequency space. Counter-clockwise direction includes angle increments. (Tracy & Resio, 1978) 31
Figure 3–2: The non-linear transfer dn/dt as a function of wavenumber. The contours are marked in units of 10^{-3} m k s units. (Webb, 1978) 33
Figure 3–3: The diagram that shows the testing process. 34
Figure 3–4: Generated input spectra (compensated) with the “Apert” value of 2. 35
Figure 3–5: The initial TSA plot for the primary examination case. 37
Figure 3–6: The comparisons with 11 frequency bands and a) 11 Angle Bands b) 7 Angle Bands c) 5 Angle Bands d) 3 Angle Bands. 38
Figure 3–7: The pair of layouts with a) 8 freq. – 7 angle bins b) 8 freq. – 5 angle bins c) 5 freq. – 7 angle bins d) 5 freq. – 5 angle bins e) 4 freq. – 7 angle bins f) 4 freq. – 5 angle bins. 39
Figure 3–8: A 2D comparison between the FBI (left), the TSA (right) and the DIA (bottom) for the first case. The TSA domain here has a 5 by 5 (angle bands and frequency bands) local scale. 41
Figure 3–9: The TSA with decreased frequency resolution. 42
Figure 3–10: The TSA with decreased angular resolution. 43
Figure 3–11: Generated input spectra (compensated) with the “Apert” value of 4. 45
Figure 3–12: The initial TSA result for this case. 46
Figure 3–13: The comparisons for the second case with 11 frequency bands and a) 9 Angle Bands b) 7 Angle Bands c) 5 Angle Bands d) 3 Angle Bands. 47
Figure 3–14: The pair of layouts with a) 8 freq. – 7 angle bins b) 8 freq. – 5 angle bins c) 5 freq. – 7 angle bins d) 5 freq. – 5 angle bins e) 4 freq. – 7 angle bins f) 4 freq. – 5 angle bins. 48

Figure 3–15: A 2D comparison between the FBI (left), the TSA (right) and the DIA (bottom) for the second case. The TSA here has a 5 by 5 local scale. 49
Figure 3–16: Generated input spectra (compensated) with the perturbation located on a closer ring to the peak..... 50
Figure 3–17: The initial TSA result for this case..... 51
Figure 3–18: The pair of layouts with a) 7 freq. – 9 angle bins b) 7 freq. – 7 angle bins c) 6 freq. – 9 angle bins d) 6 freq. – 7 angle bins e) 5 freq. – 9 angle bins f) 5 freq. – 7 angle bins..... 52
Figure 3–19: The final 2D comparison between the FBI (left), the TSA (right) and the DIA (bottom) for the third case. The TSA here has a 5 by 7 local scale. 54
Figure 3–20: The FBI run over 50 seconds with 1 second time steps. 56

TABLES

Table 1-1: JONSWAP (Υ) and Relative Peakedness (Υ_r) Values. 6

ABSTRACT

Nonlinear four-wave interactions (S_{nl}) are critical for acquiring realistic spectra needed by operational wave models. High computational demand to calculate these interactions led to an approximation method named the Discrete Interaction Approximation (DIA) to be used broadly in the major operational wave models for a long time. However, the accuracy of the DIA has been controversial since it was first introduced and more precise approximations such as the Two Scale Approximation (TSA in short) are now available. The only issue with the initial TSA`s efficiency is performing an order of a magnitude slower than the DIA in speed. This study questions the exactness of the DIA while trying to increase the competence of the TSA by making improvements on its execution time. Particularly, in this thesis, the main effort is on the local scale term of the TSA since it is the part that consumes the most time while running the code. The findings of this work imply that the TSA can improve its operation speed significantly while maintaining its accuracy with making alterations in the code. By decreasing the number of bands in the local scale it is possible to run the TSA up to 7.5 faster than its initial version.

Chapter 1: INTRODUCTION

Ocean waves play a critical role as a decision factor in a lot of fields, especially in logistics, construction and the oil industry. The dynamic structure of the waves makes people working in those fields obligated to do non-stop observations of the wave heights and directions for the sake of their projects. These observations can be translated into mathematical language concerning the instantaneous spectrum of the surface displacement (Phillips 1958). The purpose here is to display ocean waves as a random process. Considering the size of the oceans and the fluctuations in wave heights during serious climatic changes, it is not possible to keep track of waves in every desired location. Instead, estimation of wave height or direction becomes more practical than actual measurements, although historical data and remote sensing still contribute significantly toward ensuring valid estimation results. “Wave Modeling”, which is a substantial tool for wave estimation, becomes most useful when there is only an essential amount of data available for model validation.

In 1956 spectral decomposition was used in the numerical wave modeling of a sea state for the first time and focused on the North Atlantic (Gelci, Cazalé and Vassal 1957). The first operational, hemispheric wave model was introduced by the Fleet Numerical Oceanography Center; the spectral wave ocean model (SWOM) (Cardone, Pierson and Ward 1976). When the first model was introduced very little was known about the influence of mechanisms that controlled the energy distribution within spectra. Early models assumed that the wind input and wave dissipation were the only significant source terms for wave generation. It was hypothesized

that a triplet of waves would be sufficient enough to observe energy transfer between waves, however in-depth research showed that a minimum of 4 waves were required to transfer energy permanently among wave numbers. The expression for the energy flux can be interpreted in terms of quadruple interactions in which energy is transferred from three ‘active’ wave components to a ‘passive’ fourth component, which receives energy from the ‘active’ components but has no direct influence on the interaction. (K. Hasselmann 1961) These quadruple interactions (i.e. nonlinear wave-wave interactions) were among the significant source terms and parameterized in the new generation wave models which are called the 2^{nd} generation wave models.

The nonlinear wave-wave interaction model takes the input (initial conditions), processes it and at the end gives an output. This operation takes considerable time, whereas it is expected from a model to be fast and accurate. However, even with modern day computer processors, due to the complexity of the equations, calculations of the integrals that the models are based on take too much time. Because of the number of wave components in nonlinear interactions, the degree of the integral increases and as a result, more computer capacity is needed than normal to calculate it. As it will be shown in section 2, this form, called the Full Boltzmann Integral (FBI), is extremely complex and cumbersome to integrate.

Effective operating speed was an even bigger concern around the 80s than it is today considering the computer processors of the era. For this reason numerous methods were used to speed up execution times, primarily focusing on simplifications to the equations. After a while, instead of trying to calculate exact integral values, the new trend focused on “approximation methods”. As

is evident from its name, approximations are typically mathematical simplifications of the exact form that lead to answers that are close to correct. One of them, the Discrete Interaction Approximation (DIA) (Hasselmann, et al. 1985), was a major stepping stone for wave modeling and became the basis for the 3rd generation models. It owed its success to operating extremely fast in computations of the nonlinear transfer source term compared to the other methods around that time. After more than 25 years, it is still being used in the major operational wave models around the world such as WAVEWATCH III and SWAN. However its accuracy is questionable and a lot of work has been done so far to find a fast and accurate method to replace DIA.

As an alternative to DIA, the Two Scale Approximation (TSA) (Resio and Perrie 2008) has been proposed. The TSA has the potential to play a significant role in the next generation of wave models. The main logic behind this approximation is to decompose a directional spectrum into a parametric (broad-scale) spectrum and a residual (local-scale) nonparametric component (Resio and Perrie 2008). This allows the integral to be represented by broad scale interactions, local scale interactions and cross-interactions. The broad scale defines the basic structure of the interactions within the spectrum and it can be pre-computated. Degrees of freedom are defined by the number of parameters used while plotting a directionally integrated spectrum. This value increases as the number of parameters used decreases. When the number of degrees of freedom for the method`s broad scale kept similar to an actual wave spectrum`s value, perturbation term gets smaller and the method becomes more accurate. However, boosting this similarity makes it more time-consuming than expected (Perrie, et al. 2013). When the broad scale`s degrees of freedom are kept at a reduced amount the TSA`s execution time depends solely on the residual portion of the integral which are the local and cross-interactions, correspondingly.

Preliminary testing of the approximation and the comparisons with the FBI indicated that the TSA was significantly more accurate than the DIA (Resio and Perrie 2009). On the other hand, the TSA method was not fast enough to be considered as practical as the DIA method. Despite the insufficient practicality, the initial success of TSA has led to additional effort on TSA to enhance its computational speed and improve its accuracy.

One of the modifications was changing the constant $\cos^{2n}(\theta - \theta_0)$ spreading function to a function with variable spreading as consistent with conservation of momentum (Resio and Long 2011). Such conservation within a spectrum produces natural spectra which show directional spreads that are narrowest near spectral peak frequencies and broaden at both lower and higher frequencies. Another modification was defining a new reference spectrum for the broad scale term (Bender, et al. in progress). The new basis (Figure 1-1) represents the link between JONSWAP and f^{-4} spectrums for different peakedness values. Its parameters are consistent with dynamics and observations made over time besides they are more robust in at demonstrating non-linear fluxes compared to the initial version of the TSA.

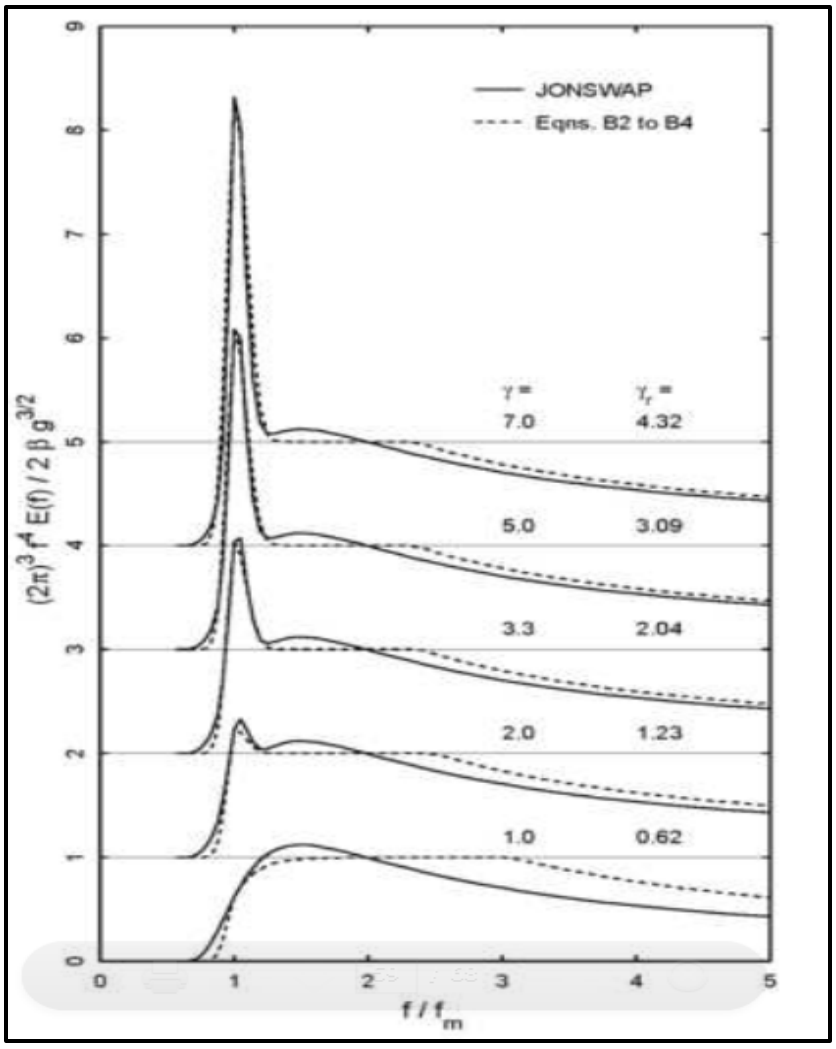

Figure 1–1: New Spectra used in the Modified TSA.

Table below shows the relationship between JONSWAP and relative peakedness values for 5 different cases.

Table 1-1: JONSWAP (ϒ) and Relative Peakedness ($ϒ_r$) Values.

$ϒ_r$	4.32	3.09	2.04	1.23	0.62
ϒ	7	5	3.3	2	1

The following equation shows the relationship for the new energy spectrum:

$$E\left(f/f_m, \theta-\hat{\theta};\, \beta, \gamma_r\right) = \frac{1}{f} E\left(f/f_m;\, \beta, \gamma_r\right) D\left(\theta-\hat{\theta}; f/f_m, \gamma_r\right) \quad (1\text{-}1)$$

Remaining modifications are going to be focus of this work, in particular examining the concept of varying the domain of the initial TSA`s local scale. In addition to limiting the size of the domain of the local scale, decreasing the resolution of the frequency bands and angle bands will be investigated. Further details and outcomes of this modification will be examined in the following chapters. Apart from completed and ongoing modifications another revision is operating the TSA on a continuous basis rather than a discretized basis. The reason for that is seeing that a continuous peak frequency provides a better estimate towards S_{nl} then the previous discretized approach.

These modifications will be tested with different sorts of cases to demonstrate their efficiency. It is certain that the modifications will boost up the speed of the TSA, the crucial part is examining whether these alterations affected the precision of the technique or not by using different scenarios. Three of these tests are going to be adding perturbation to the high frequency part of the input spectrum. This test reflects a real-life case involving a swell and will show that even a

small perturbation in the energy spectra can affect the graph of the S_{nl} significantly. The third one of these tests will be using a “double peaked spectrum” which is equivalent of a sudden wind shift in reality. It can be considered as an extreme perturbation case compared to the first two tests. Additionally it will show the need for a second scale term in the TSA after analyzing the result. Remaining test is examining the “relaxation”. Relaxation tests will help to see how fast a perturbed spectra goes back to equilibrium.

This thesis focuses on optimizing the TSA method for calculating the S_{nl} source term. Following this introduction, a discussion of the overall methodology used here will be introduced. After that, there are going to be modifications made for the TSA and discussions and conclusions regarding the results obtained.

Chapter 2: METHODOLOGY

In this thesis work there will be three main components actively used that were developed in the FORTRAN environment; the first one is the DIA, based on a FORTRAN code developed as a part of this thesis. The FBI was used for comparison purposes and an independent TSA is the actual code going to be optimized by the combination of two different methods.

The following sections provide further detailed information on the energy transfer, the FBI and the TSA.

2.1. Energy Transfer between Waves and the Full Boltzmann Integral

Ocean waves are generated by winds which vary in both time and space. A non-dynamic or constant wind can only be observed in some exceptional or small scale occasions or under idealized conditions. This situation requires a general form for the spectral density $E = E(f, \theta)$ to be rewritten in a form that includes time (t) and space(x and y coordinates) parameters:

$$E(f, \theta) = E(f, \theta; x, y, t) \tag{2-1}$$

It is apparent that ocean surface consists of many spectral components propagating from various directions. Even though the typical approach is to analyze a group of waves as a whole, energy

density of each wave component (f, θ) can be obtained by integrating an energy evolution equation while propagating with the group velocity along a wave ray (Holthuijsen 2007):

$$\frac{dE(f,\theta;x,y,t)}{dt} = S(f,\theta;x,y,t) \tag{2-2}$$

Change in x and y coordinates here denotes group velocity along a wave ray, whereas the source term on the right hand side of the equation consists of three components: wind input (S_{in}), non-linear interactions (S_{nl}) and white capping (S_{wc}), respectively.

$$S = S_{in} + S_{nl} + S_{wc} \tag{2-3}$$

The integration of the source term does not only depend on a single wave ray but on all the wave rays crossing through this specific wave ray. This situation leads to a calculation with unknown parameters, which is not soluble. One of the best possible ways to examine the energy density of each wave component is to analyze the water surface as grid cells consisting of x and y coordinates. It is possible to keep track of the energy change in each cell that is caused by local generation or import of energy using this methodology. The spectral energy balance can be represented by the following equation (Holthuijsen 2007):

$$\frac{\partial E(f,\theta;x,y,t)}{\partial t} + \frac{\partial c_{g,x}(f,\theta;x,y,t)}{\partial x} + \frac{\partial c_{g,y}(f,\theta;x,y,t)}{\partial y} = S(f,\theta;x,y,t) \tag{2-4}$$

Among the source terms, this paper`s focus is on the non-linear wave-wave interactions. These interactions manage the energy transfer between higher and lower frequencies by playing an active role around mid-frequencies. They are important for developing realistic spectra required by operational wave models. As it was stated above, a minimum of 4 waves are required for a permanent energy transfer.

Waves are represented by wave-number vectors so these 4 interacting waves can be shown by k_1, k_2, k_3 and k_4. In deep water, this energy transfer can occur between two pairs of waves which creates a diamond pattern and this situation can be presented by resonance conditions:

$$f_1 + f_2 = f_3 + f_4 \tag{2-5}$$

$$\vec{k}_1 + \vec{k}_2 = \vec{k}_3 + \vec{k}_4 \tag{2-6}$$

The equation to calculate these interactions, a Boltzmann Integral, can be seen in the following form (K. Hasselmann 1961):

$$\begin{aligned} S_{nl4}(\vec{k}_4) = & \iint \iint T_1(\vec{k}_1, \vec{k}_2, \vec{k}_1 + \vec{k}_2 - \vec{k}_4) E(\vec{k}_1)\, E(\vec{k}_2) E(\vec{k}_1 + \vec{k}_2 - \vec{k}_4) d\vec{k}_1 d\vec{k}_2 \\ & - E(\vec{k}_4) \iint \iint T_1(\vec{k}_1, \vec{k}_2, \vec{k}_4) E(\vec{k}_1)\, E(\vec{k}_1) d\vec{k}_1 d\vec{k}_2 \end{aligned} \tag{2-7}$$

Here, the first integral is considered as “passive” part whereas the second integral is the “active” part, with respect to whether they depend on E (k_4) or not. On the other hand, the rate of change

of energy density at a point within a spectrum can be written as an integral of the T (k_i, k_j) which denotes the rate of action transfer between the i^{th} and j^{th} wave numbers (Webb 1978):

$$\frac{\partial n(k_1)}{\partial t} = \int_0^{2\pi} \int_0^{\infty} T\,(k_1, k_3)\; dk_3\, k_3\, d\theta \qquad (2\text{-}8)$$

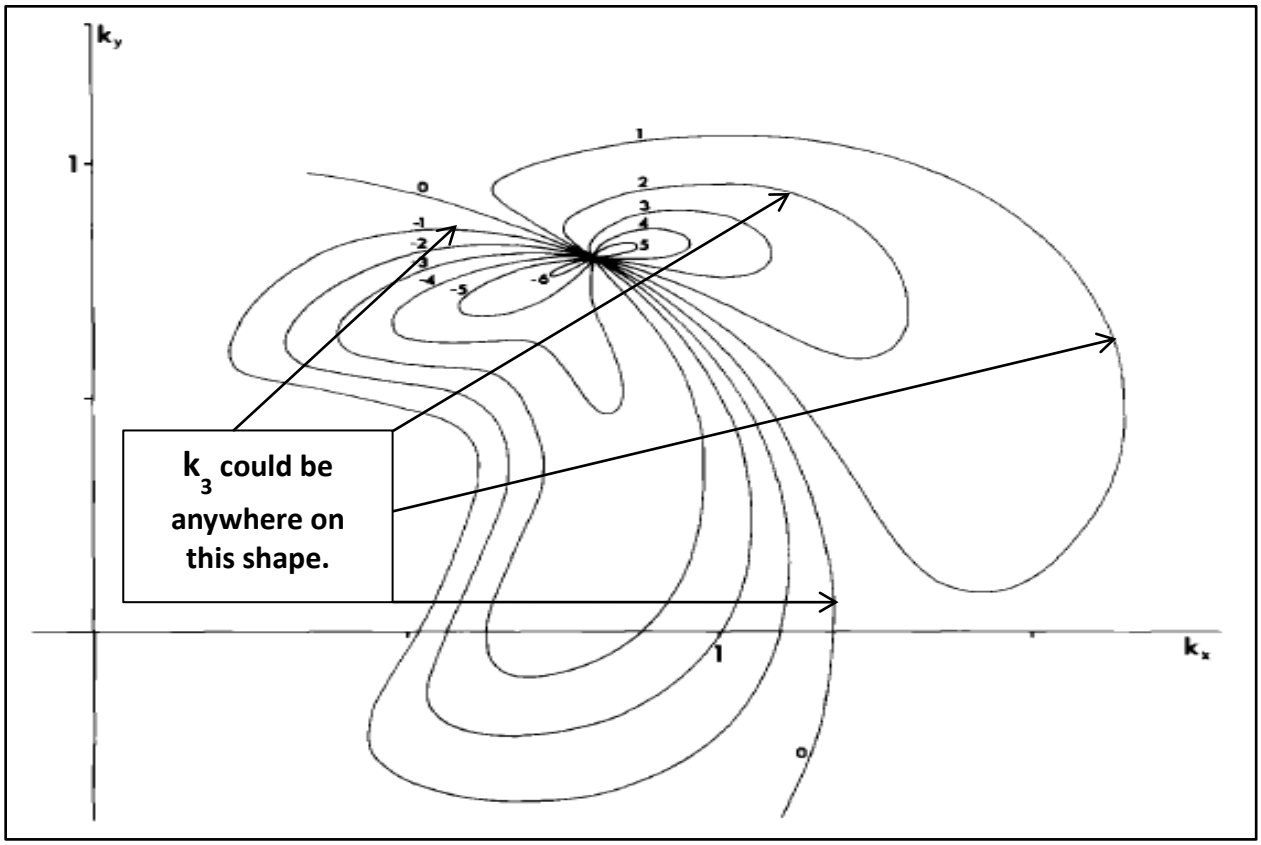

Figure 2–1: The pumped transfer Tp (k_1, k_3) for k_1 (0.8, 0.8) (Webb 1978)

Figure 2-1 represents how much energy is transferred into and out of a specific value of k_1 on a wave number space. It should be noted that only k_1 is pre-defined, however k_3 could be

anywhere on the shape. Negative and positive numbers show that energy transfers are coming into $k_1$from lower wave numbers (or frequencies) and moving to higher wave numbers (or frequencies) for this specific condition. An expanded form of the transfer function which includes contour integral is:

$$T(k_1, k_3) = 2 \oint D(k_1, k_2, k_3, k_4)\, C(k_1, k_2, k_3, k_4) \left|\frac{\partial W}{\partial n}\right|^{-1} \delta(|k_1 - k_4| - |k_1 - k_3|)ds \tag{2-9}$$

Where δ is the Delta function, C is the coupling coefficient and D is a density function that consists of action densities:

$$D(k_1, k_2, k_3, k_4) = n(k_1)n(k_3)[n(k_4) - n(k_2)] + n(k_2)n(k_4)[n(k_3) - n(k_1)] \tag{2-10}$$

2.2. The Two Scale Approximation and The Discrete Interaction Approximation

2.2.1. The DIA

Equation 2-10 is the most time-consuming part during the calculation of the transfer integral. This is the reason that approximations or assumptions are typically used for this part of the integral in the Discrete Interaction Approximation.

The major aspects of the nonlinear transfer can be represented by finding the interactions between the wavenumbers which are closely located on wave number space. Following this first step, finding some similarities between the interactions would have been produced some useful results. After some experimentation it was found that the exact nonlinear transfer could in fact be well simulated by just one mirror-image pair of intermediate-range interaction configurations. (Hasselmann, et al. 1985). The DIA uses this and implements an additional Delta function into the transfer Integral ($k_1 = k_2$):

$$\frac{\partial n(k_1)}{\partial t} = \int_0^{2\pi} \int_0^{\infty} T(k_1, k_3)\delta(k_1 - k_2)\, dk_3\, k_3\, d\theta \tag{2-11}$$

$$\delta(k_1 - k_2) = 1 \quad \text{when} \quad |k_1 - k_2| \leq \in \quad (\in \approx 0) \tag{2-12}$$

Equation 2-11 form helped the transfer integral to conserve action, energy and momentum while decreasing the calculation load. In addition to the $k_1 = k_2$ assumption, it was assumed that k_3 and k_4 wavenumbers lie at a certain angle to the wave number k:

$$\overrightarrow{k_3} = 0.75\overrightarrow{k_1} \tag{2-13}$$

$$\overrightarrow{k_4} = 1.25\overrightarrow{k_1} \tag{2-14}$$

These two assumptions created a shape which is called a “Figure-8 Shape” on wave number space (see Figure 2-2). It helped to simplify calculations by allowing the discretized representation.

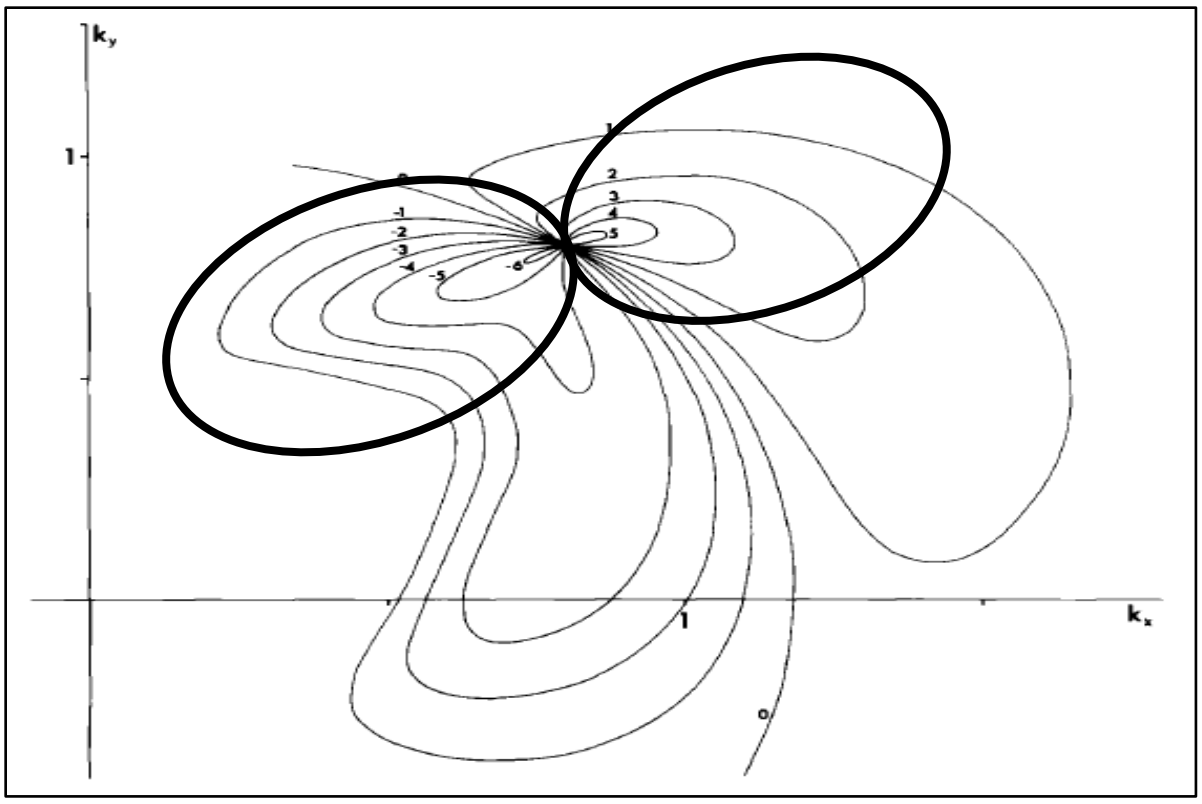

Figure 2–2: Figure-8 Representation on Wave Number Space.

2.2.1.1 Comparisons between the DIA and the FBI

Speed is only one of the factors that are distinctive on the usefulness of a method. Another critical factor is accuracy. When the final spectral shape of a 3rd generation model's output is not accurate, the general approach has been to calibrate the model by using coefficients. Coefficients affect the magnitude, as well as the shape of a nonlinear source term. However representing the physics of the interactions is not possible without having the correct form. So, coefficients only have a limited use. Consequently, adopting the correct form of the integral is vital.

The most reliable way to check accuracy of a program is to compare it with the FBI (i.e. the actual integral) with the same input spectra and conditions. In the following two subsections this comparisons will be made in one and two dimensional (1D & 2D) environments. First set of comparisons are going to be in 1D scale.

2.2.1.1.a. One Dimensional Comparisons

These comparisons include only magnitude and frequency information and they provide an essential overview on the level of accuracy before proceeding to the next set of matches in the 2D environment.

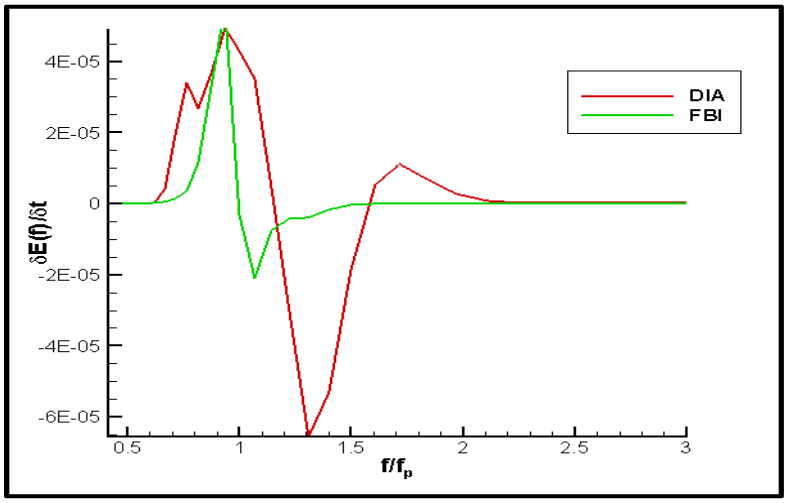

Figure 2–3: The DIA vs. The FBI for relative peakedness of 2.04

The DIA in figure 2-3 above is the calibration case, which means coefficient(5.5×10^{14}) is used to calibrate referencing the FBI on the same peakedness level. It shows a good fit at lower frequencies but a strong negative lobe at higher frequencies. It was hypothesized by Hasselmann

et al. (1985) that this feature is less important for a satisfactory reproduction of wave growth than the correctly simulated form of the positive lobe, which controls the rate at which the spectral peak shifts towards lower frequencies.

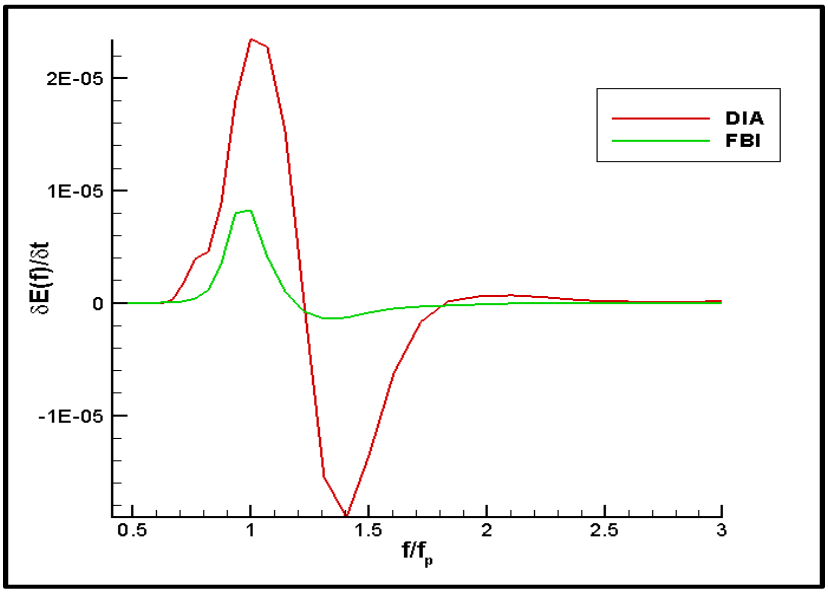

Figure 2–4: The DIA vs. The FBI for relative peakedness of 0.62

Figure 2-4 is a case where peakedness is low. Here the DIA is not only working inefficiently at the negative lobe but also makes an over prediction at how much flux is going in at the front face of the spectrum. Thus, the reasonable fit of the low-frequency lobe of the DIA for wave growth is only achieved locally relative to peakedness by calibration to that case.

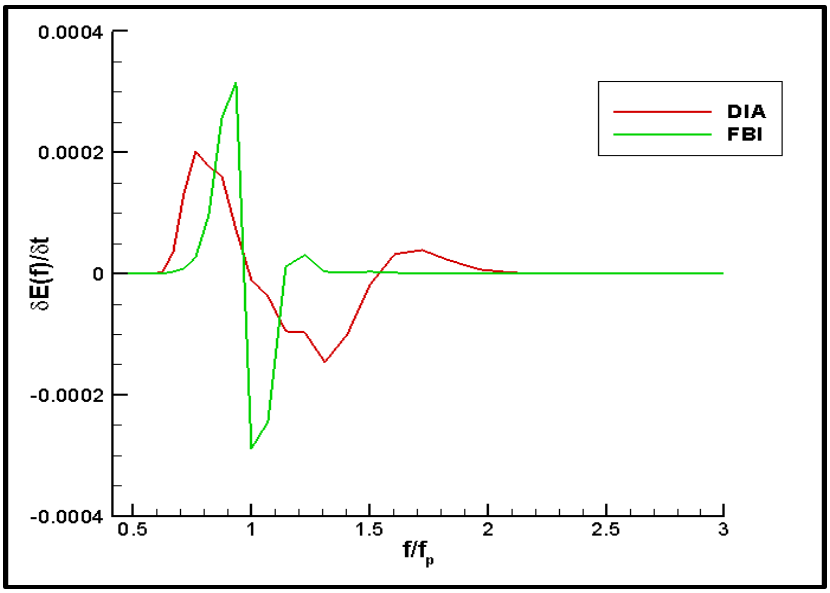

Figure 2–5: The DIA vs. The FBI for the relative peakedness of 4.32

In the figure 2-5 relative peakedness is 4.32 and it is the maximum value amidst the comparisons. In opposition to the first two cases, as it can be seen in this figure, the DIA under predicts the actual spectra values around the negative lobe as well as the front face of the spectrum. Furthermore, compared to the FBI, the peak value is shifted slightly to the lower frequencies of the spectrum .

2.2.1.1.b. Two Dimensional Comparisons

Two dimensional comparisons help understanding the level of accuracy of the method by visualizing the angular spreading besides providing frequency information. Following figures are used here to show discrepancies between the DIA and the FBI in a better way with respect to the one dimensional.

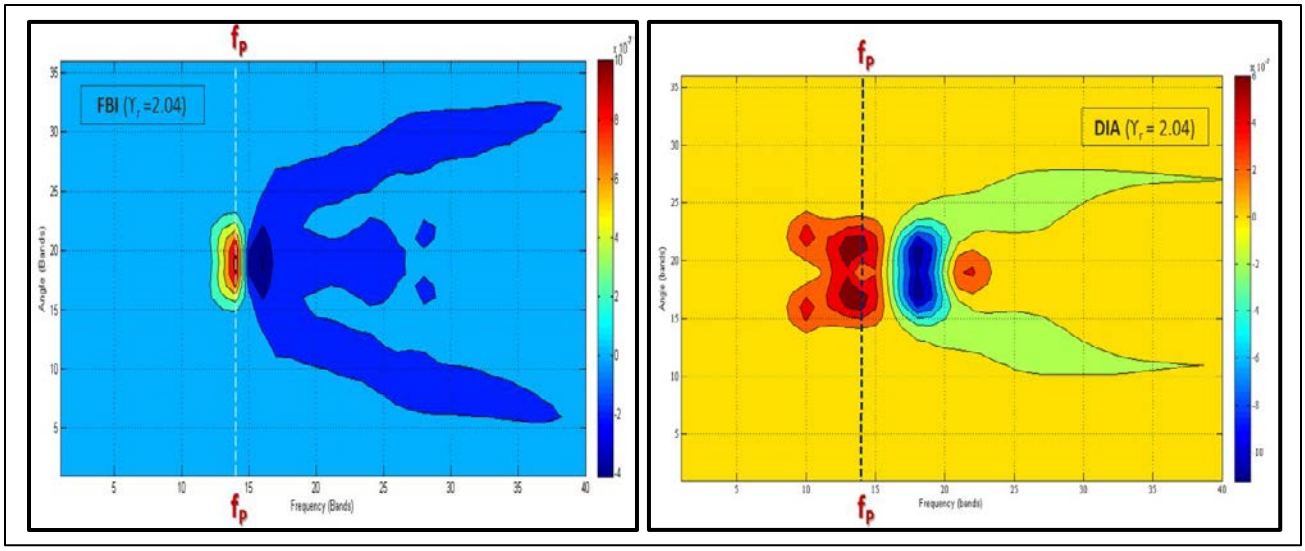

Figure 2–6: 2D Comparison for Relative Peakedness of 2.04

Figure 2-6 is the calibration case once again. In the 1D comparison the DIA seemed to have a good fit with the FBI, despite its inefficiency at the negative lobe. However, it looks very jagged compared to the FBI when viewed in two dimensions.

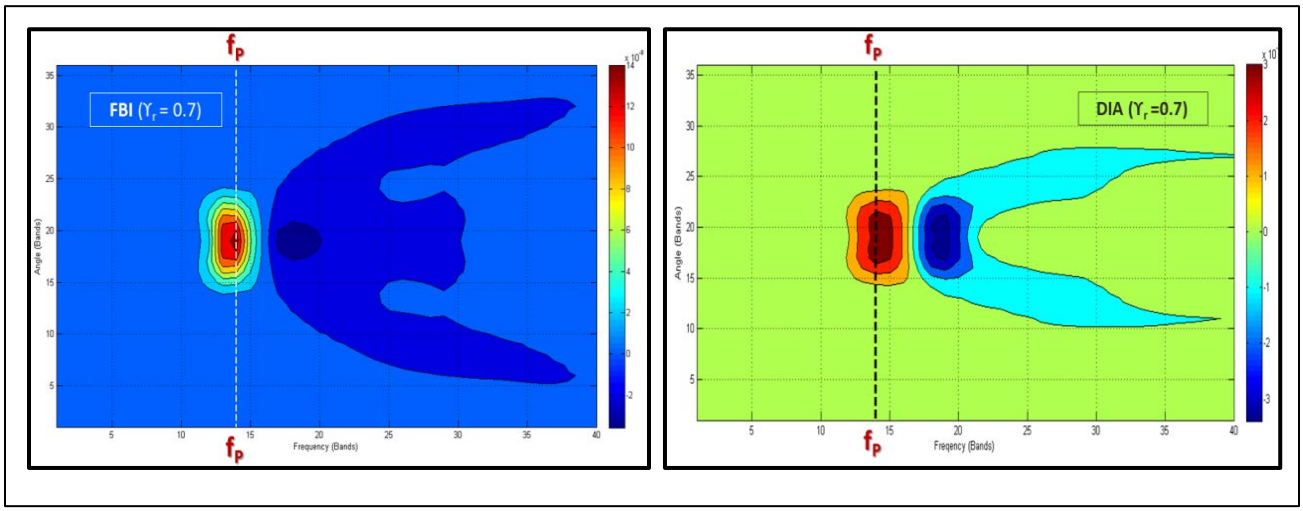

Figure 2–7: 2D Comparison for Relative Peakedness of 0.62

The DIA is smoother and less jagged in the figure 2-7 than in the previous figure since the peakedness is now reduced. Also it is somewhat better in representing the direction in that peak values are consistent, but on the other hand, the magnitude is not good as it has already noted.

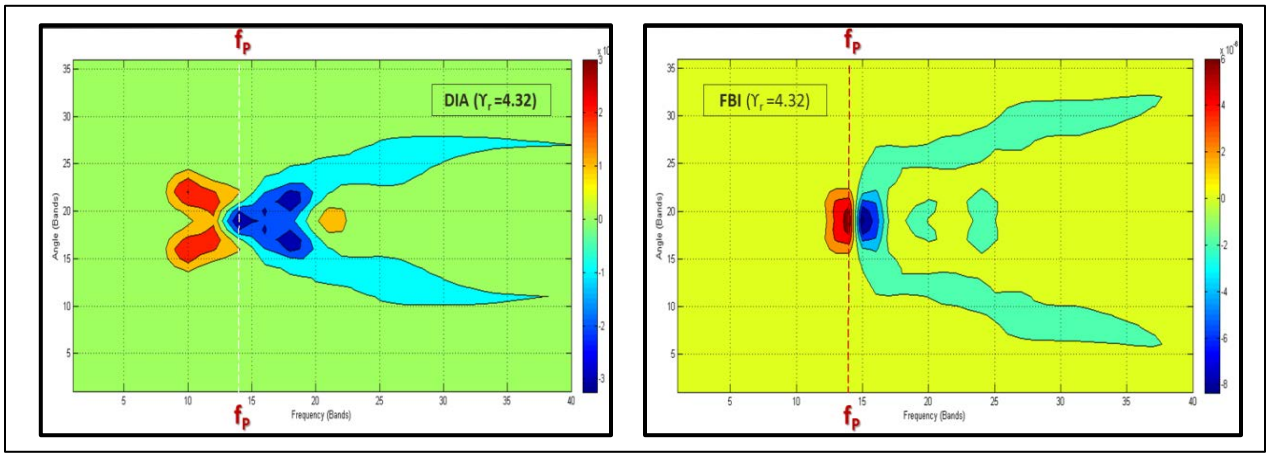

Figure 2–8: 2D Comparison for Relative Peakedness of 4.32

Figure 2-8 shows the last comparison with the highest relative peakedness value. This time not only the magnitude is different but also the DIA distributes the energy more unevenly. These results shown are for simple cases. In the real life complicated scenarios the results would get much worse than this.

The practical consideration within the DIA prevented it from representing the general interactions space, affected the accuracy of the model primarily because the integral in the DIA does not have the same form as the FBI. Even in the initial paper proposing the DIA, it is stated that the DIA will undoubtedly need to be modified and improved as further experience is gained in the operation of the model. (WAMDI Group 1988)

2.2.2. The TSA

The TSA starts with treating the directional spectrum in parametric (broadscale) and residual(local scale) components: (Resio and Perrie 2008).

$$n_i = \hat{n}_i + \grave{n}_i \tag{2-15}$$

In this equation $\hat{n}_i$ is the parametric term and $\grave{n}_i$ is the perturbation term.The transfer integral consists of broad scale interactions(B), local scale interactions(L) and cross-interactions(X) after mounting equation 2-15 into equation 2-9, so the source term can be described as:

$$S_{nl}(f,\theta) = B + L + X \tag{2-16}$$

The broadscale term can be pre-computated since it contains known parameters in it, to reduce the computational burden during calculations. L and X represents perturbations and accepted as Local Scale terms together which covers some negligible parameters . Thus, in order to decrease some load on the integral and obtain operational speed, further calibrations such as neglecting the terms including $\grave{n}_2$ and $\grave{n}_4$ in the local and cross-interactions is needed . The reason for that is they contribute less to the total transfer than the other terms. This also leaves only 8 triplets in the local scale as will be shown here.

Following these alterations, final form of the equation is (Resio and Perrie, 2008):

$$\frac{\partial n_1}{\partial t} = B + \iint \oint N_*^3 \, C \left|\frac{\partial W}{\partial n}\right|^{-1} \, ds \, dk_3 \, k_3 \, d\theta \tag{2-17}$$

Where N_*^3 is given by;

$$N_*^3 = (\grave{n_1}\grave{n_3})(\hat{n}_4 - \hat{n}_2) + (\hat{n}_1\grave{n_3})(\hat{n}_4 - \hat{n}_2) + (\hat{n}_3\grave{n_1})(\hat{n}_4 - \hat{n}_2) + (\grave{n_3} - \grave{n_1})(\hat{n}_4\hat{n}_2) \tag{2-18}$$

2.2.3. Benchmarking the Calculation Speeds of the TSA and the DIA

Local Scale of the equation can be shown with total summation symbols since it is an integral:

$$\sum_{i=1}^{N_k}\sum_{j=1}^{N_\theta}\{(\grave{n_3} - \grave{n_1})\Lambda_d + (\grave{n_1}\grave{n_3} + \hat{n}_1\grave{n_3} + \hat{n}_3\grave{n_1})\Lambda_p\} k_3\overline{\Delta k} \tag{2-19}$$

The Number of operations in a single summation includes 6 multiplications and 3 addition-subtractions. The two matrices pumping (Λ_p) and diffusive (Λ_d) involve two broad scale terms,$\hat{n}_2$ and $\hat{n}_4$, coupling coefficient(C) and $\left|\frac{\partial W}{\partial n}\right|^{-1}$ as the energy conservation term. They are pre-computed and do not affect the calculation speed.

$$\Lambda_p = \oint \; C \left|\frac{\partial W}{\partial n}\right|^{-1} (\hat{n}_4 - \hat{n}_2) ds \Delta\theta \tag{2-20}$$

$$\Lambda_d = \oint C \left|\frac{\partial W}{\partial n}\right|^{-1} (\hat{n}_4 \hat{n}_2) ds \Delta\theta \tag{2-21}$$

In the initial TSA code there are 17 angle bands (N_θ) and 11 frequency bands (N_f), thus total number of summations in one time step is: 17 x 11=187 So the total number of operations in one time step which defines computational speed is: 187 x (6+3) = 1683.

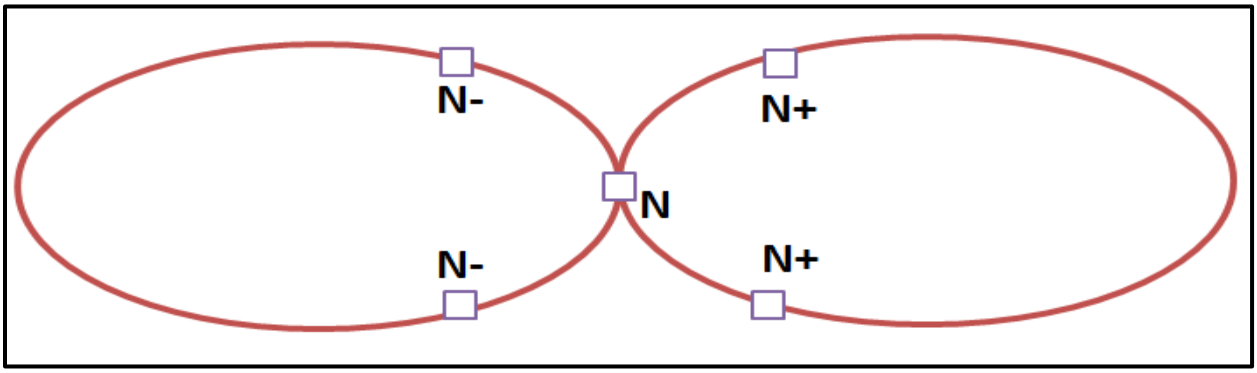

Figure 2–9: Figure-8 Shape for Energy Transfer Integral

On the other hand, the Discrete Interaction Approximation approach focuses on the Figure-8 shape which looks like the combination of two ellipses that occurs after adding a delta function to the transfer integral and assuming all the energy transfer is happening only on this line. A quick review of equation 2-8 implies that there should be a unit area defined by the dimensions k_x and k_y for an energy transfer to occur on the wave number space, if there is no unit area the transfer goes to zero. Formally, the integral of an ellipse (or any line in this space) is zero since a line has only one dimension and therefore has no integration area as required to produce a finite results in combination with the dimensionality of the integrand with the FBI. In order to calculate

(or approximate) the integral there should have been some infinitesimal (but finite size) boxes to be added (figure 2-9).

This shape is centered on an actual grid point which has dimensions of angle and frequency, center box is accepted to be a point with a known action density. As a result of another supposition in the DIA, the position of the remaing 4 grid cells are predetermined and each of them are examined individually. The boxes on the left hand side are (N-) and the ones on the other side are (N+). The purpose here is to find real energy transfer points which are located inside of these 4 rectangle areas by using interpolation technique since the positions are predetermined. In the figure 2-9, not just the ratios "λ" and "k" but also the action densities at each of the 4 corner points N_A, N_B, N_C and N_D of the rectangle are known. So the most important step would be to find the action density inside the rectangle.

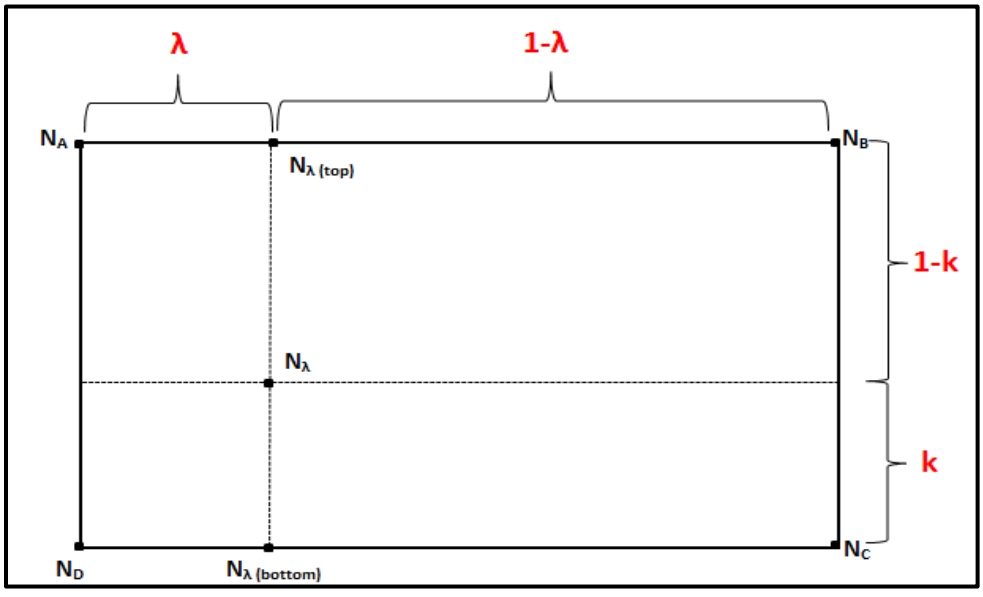

Figure 2–10: An individual grid cell for the DIA.

In order to find action density N_λ, following interpolations must be made:

$N_{\lambda\,(top)} = N_A\,(1-\lambda) + N_B\,(\lambda)$ (1 add.-sub.) (2 multiplication)

$N_{\lambda\,(bottom)} = N_C\,(1-\lambda) + N_D\,(\lambda)$ (1 add.-sub.) (2 multiplication)

$N_\lambda = N_{\lambda\,(bottom)}\,(1-k) + N_{\lambda\,(top)}\,(k)$ (1 add.-sub.) (2 multiplication)

TOTAL = (3 add.-sub.) (6 multiplication)

At the end there are a total of 9 operations for a single grid cell and this operation should be completed for the remaining 3 boxes as well.

(3 add.-sub.) (6 multiplication) x 4 grid cells = (12 add.-sub.) (24 multiplication)

After the action densities are found for all of boxes the final step is finding action density change or the transfer by using the following equation:

$$\frac{\partial}{\partial t}\begin{vmatrix} N \\ N_+ \\ N_- \end{vmatrix} = \begin{vmatrix} -2 \\ +1 \\ +1 \end{vmatrix} Cg^{-8}f^{19}[N^2(N_+ + N_-) - 2N(N_+N_-)]\Delta k \qquad (2\text{-}22)$$

In this equation there are 3 multiplications and 2 addition-subtractions. So for one matrix there are a total of 27 multiplications and 14 addition-subtractions. Multiplying this number with three matrices (27+14) x 3 = 123 is the total number of operations in the DIA method.

Comparing the number of operations in the TSA (1683) and the DIA (123), proportion of the speed of the local scale to the DIA method is 1683/123 ~ 13.5. In other words, the DIA method is about 13.5 times faster than the initial TSA.

2.2.4. Performance Benchmarking between the TSA and the DIA

The DIA has an important operational advantage compared to the TSA by operating 13.5 times faster. Nevertheless, as it was mentioned before, speed is not the only factor that defines the effectiveness of a model. The shape of the final spectrum that a model produces must reflect similarities between the one achieved using the actual method since it provides vital information required in accurate wave modeling. Any discrepancy in the shape will cause more bias on later spectral outputs considering the fact that after embedding the first input, models recursively use their own output for the next time step. For this reason, 1D and 2D comparisons between the 3 methods are included. The accuracy of the DIA is not the main focus of this thesis paper, thus, plots of a previous work which used actual site data collected using wave sleds in Currituck Sound, North Carolina are used.

Figure 2-11 shows the plots for 4 cases using 3 models on different positions and conditions. In all cases the DIA does not represent the spectral shape well and looks very jagged. The TSA does a much better job representing positive and negative lobes of the transfer function and appears to be smoother.

Figure 2-12 includes 2D results in two different pairs for 3 procedures. Since these outputs are obtained by using actual site data, as opposed to the 2D comparisons in the section 2.2.1.1.a these results are asymmetrical and there are discontinuities along the plot. Despite these complexities, the TSA operates much more reasonably than the DIA which produces quite chaotic plots. The reason behind including these comparisons in this paper is to show that the TSA works very precisely compared to the DIA. The modifications on the following chapter will focus on providing a boost in speed while maintaining its accuracy and eventually lead the TSA to become more operational than its initial version.

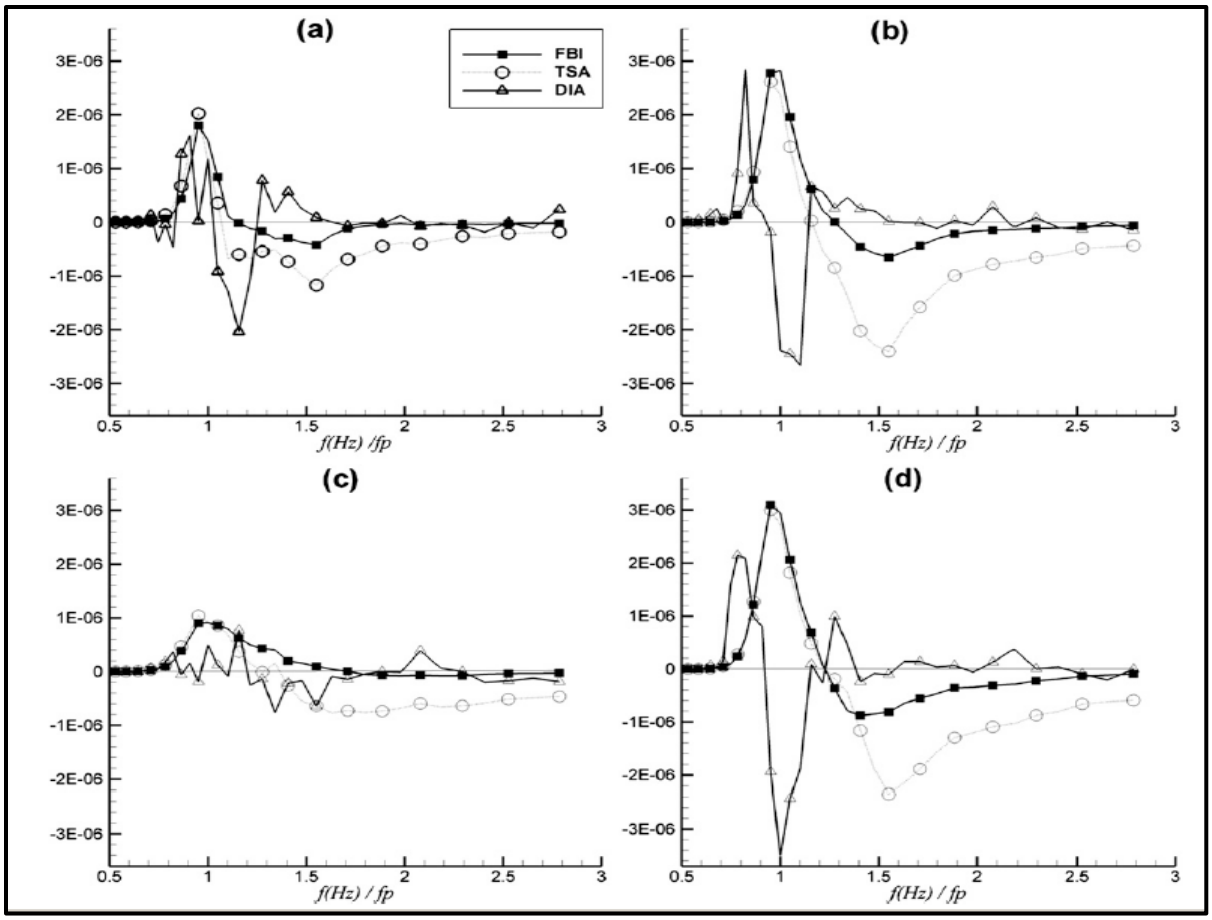

Figure 2–11: Comparisons of 1D nonlinear transfer (m2 Hz-1 s-1) for FBI, TSA, and DIA using Currituck Sound data for different locations called a, b, c and d respectively. (Resio and Perrie 2009)

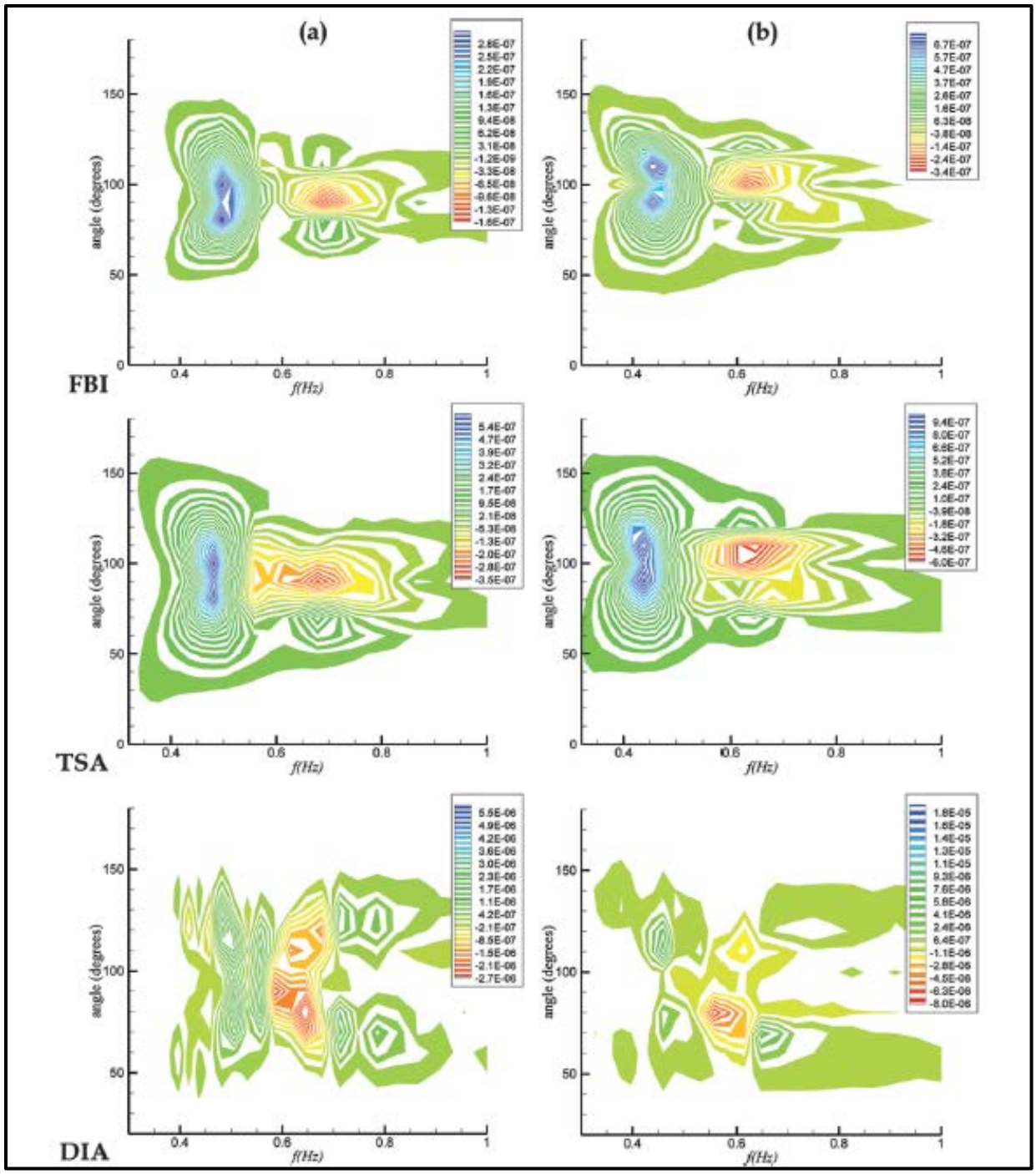

Figure 2–12: The 2D results (m^2 Hz^{-1} s^{-1}) using Currituck spectra for the FBI, the TSA, and the DIA for two different cases called “a” and “b”. (Resio and Perrie 2009)

Chapter 3: MODIFICATIONS

The serious operational speed difference between the TSA and the DIA requires some modifications to be made in the TSA method. The main challenge here is to perform these changes without significantly affecting the accuracy of the model. Before going into detail of the modifications, it would be worthwhile to mention the tools used.

3.1. Programs used

As was mentioned before, codes written in FORTRAN are the base tools for the majority of this thesis work. The testing process starts with generating various types of spectra by using the program "Specgen". The end products of this program are energy densities that include perturbation. Thus, the end product (i.e. the total energy density) consists of broad scale and perturbation components. These two components and their total energy density can be converted into action density with the help of the Jacobian that can be seen in the following equation:

$$\mathrm{N}(\mathrm{k},\theta) = \mathrm{E}(\mathrm{f},\theta)\ \frac{C_g}{2\pi\omega} \tag{3-1}$$

C_g is the group velocity and ω is the angular frequency here. Jacobians are crucial to help keeping consistency between or within the programs by assuring they are using the same basis such as wave number or frequency. After converting total and broad scale energy into action

densities these outputs are used by both the FBI and the TSA. The underlying cause using both of these densities in the FBI is to gain two sets of outputs.

The first set is the ideal result that is obtained by running the program by using the total action density input. This set of output includes the actual S_{nl}, which is going to be used in testing. The second set of output is obtained by using the broad scale action density input. This time the output consists of the broad scale S_{nl}, pumping Λ_p and diffusive Λ_d matrices. These are used as input variables for the TSA code, as well as total and broad scale action densities.

The last step is running the TSA with the above mentioned inputs. The end product of this process is another total S_{nl} that should show resemblance to the actual result. It is a recursive operation with different input spectras and repeated after each modification made to the initial TSA. The following two subsections give more precise information on the Specgen and the TSA codes.

3.1.1. The Specgen Program

This program can produce various one (frequency only) and two dimensional (frequency and angle) spectral shapes such as JONSWAP with variable spreading of the energy, f^{-4} spectral form with "random" errors i.e. perturbation. Our testing process requires spectrums with perturbations; because of this the Specgen program becomes quite useful.

This program requires input parameters including peak frequency, frequency multiplier, peakedness, number of frequency and angle bands. In addition to these it allows user to “place” a

negative or positive perturbation with a desired magnitude on any specific frequency band. It also allows an option to use specific angular and frequency spreading coefficients. The Specgen program produces broad scale and perturbation scale energy densities with frequency basis.

3.1.2. The TSA

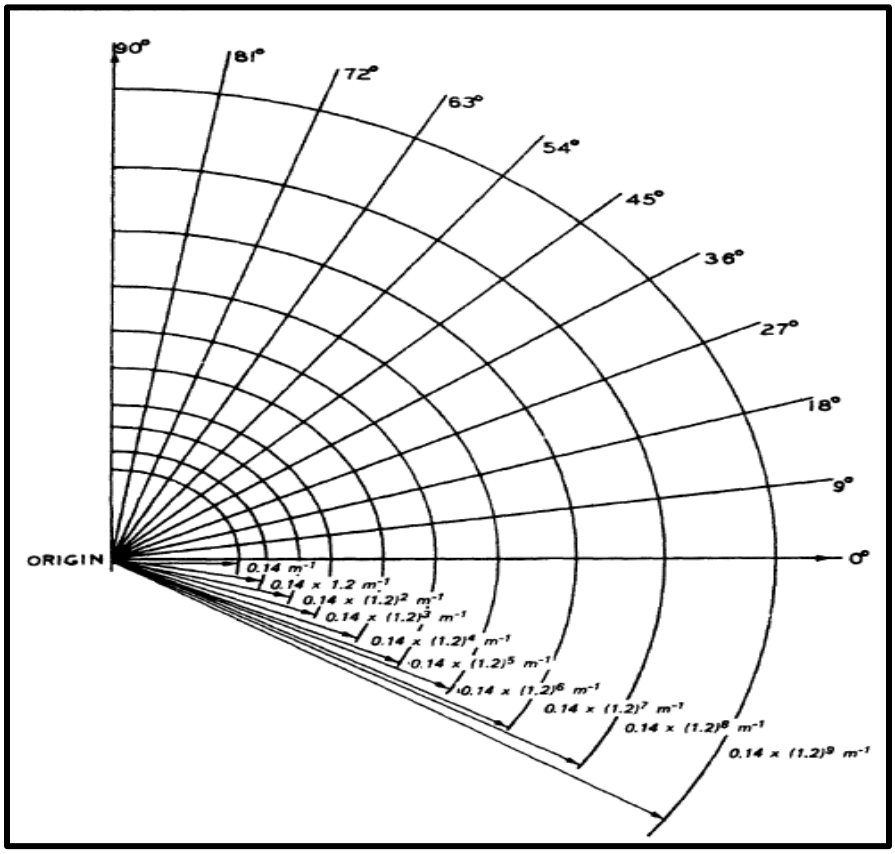

Figure 3–1: Specification of Integration Grid. Radius represents wave number or frequency space. Counter-clockwise direction includes angle increments. (Tracy and Resio 1978)

Because optimizing the TSA is the main focus of this paper, an independent and simplified TSA was developed as a part of the thesis. The simplified TSA model has 5 input data sets; three (3)

(broad scale S_{nl}, pumping Λ_p and diffusive Λ_d matrices) come from the FBI and two (2) (broad scale and total action densities) come from Specgen. It also includes two functions that support to define terms required during execution of the program. The first function uses Pade approximation to find inversion of the linear wave dispersion relation; by other words it uses frequency and depth data in order to find wave number. Wave number must be determined to find phase speed. The second one computes group velocity from frequency, depth and phase speed. Group velocity is a critical factor used actively finding Jacobians.

The TSA has to reference angle and frequency parameters from both broad and local scale to accomplish calculations. Because of this, pumping and diffusive matrices have five dimensions since they are referenced by general and local scale frequency as well as their peakedness level. The broad scale consists of 71 frequency and 36 angle bands which also specifies the general integration grid as it can be seen from the Figure 3-1. This whole operation intends to find the transfer between k_1 and k_3 wave number vectors.

Choosing 17 by 11 grid subset for local scale stems from the assumption that the TSA calculation is needs to cover the entire domain of transfers shown on figure 3-2. However the significant contributions will be shown to be representable by a much reduced area.

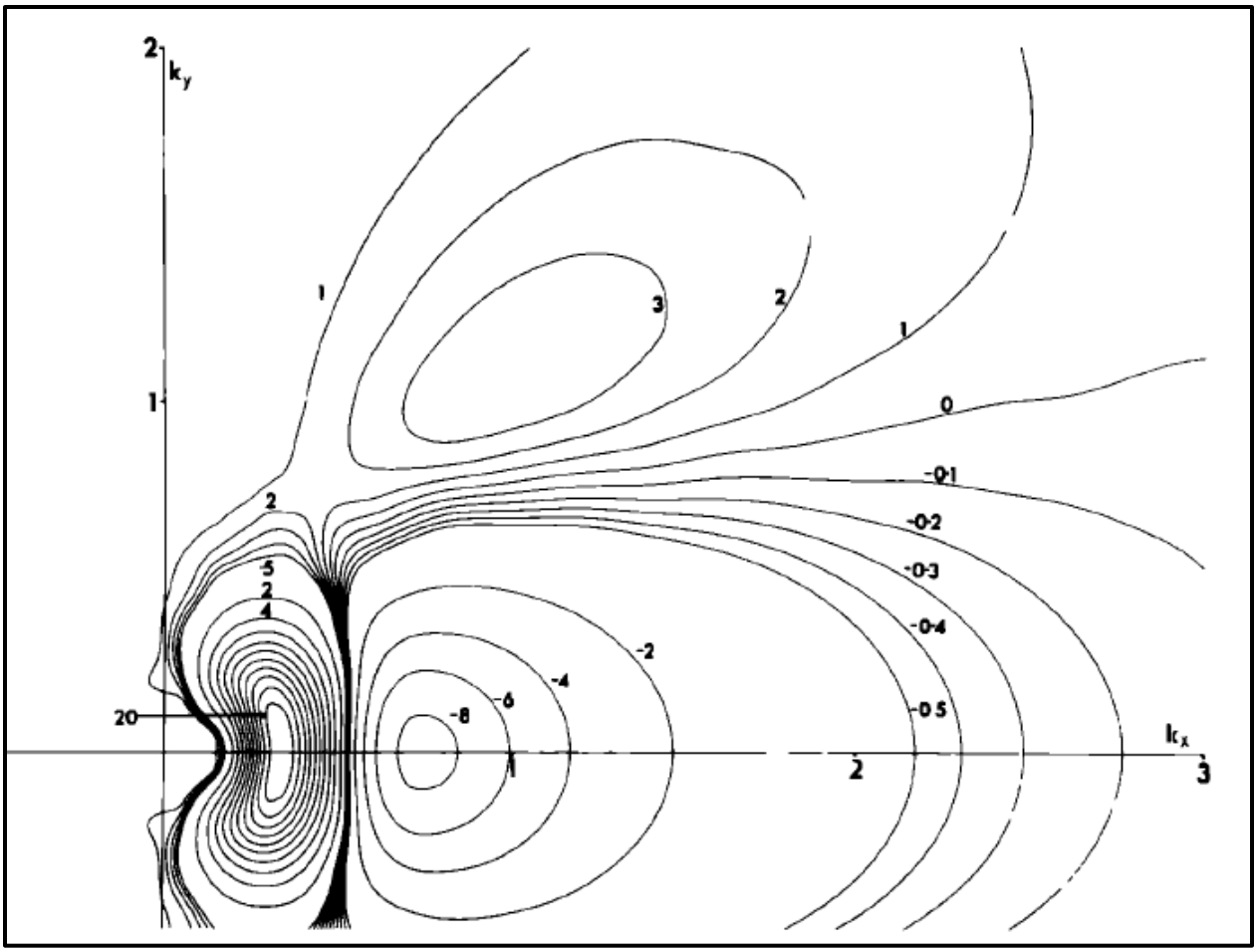

Figure 3–2: The non-linear transfer dn/dt as a function of wavenumber. The contours are marked in units of 10^{-3} m k s units. (Webb 1978)

The whole execution process is illustrated on the following diagram. Ovals are the main programs and rectangle boxes are input or output values. Arrows show which program have which input and what output they produce. Long dashed lines show the first way of calculations and first set of the outputs whereas dashed dotted lines show the second way and set of the execution.

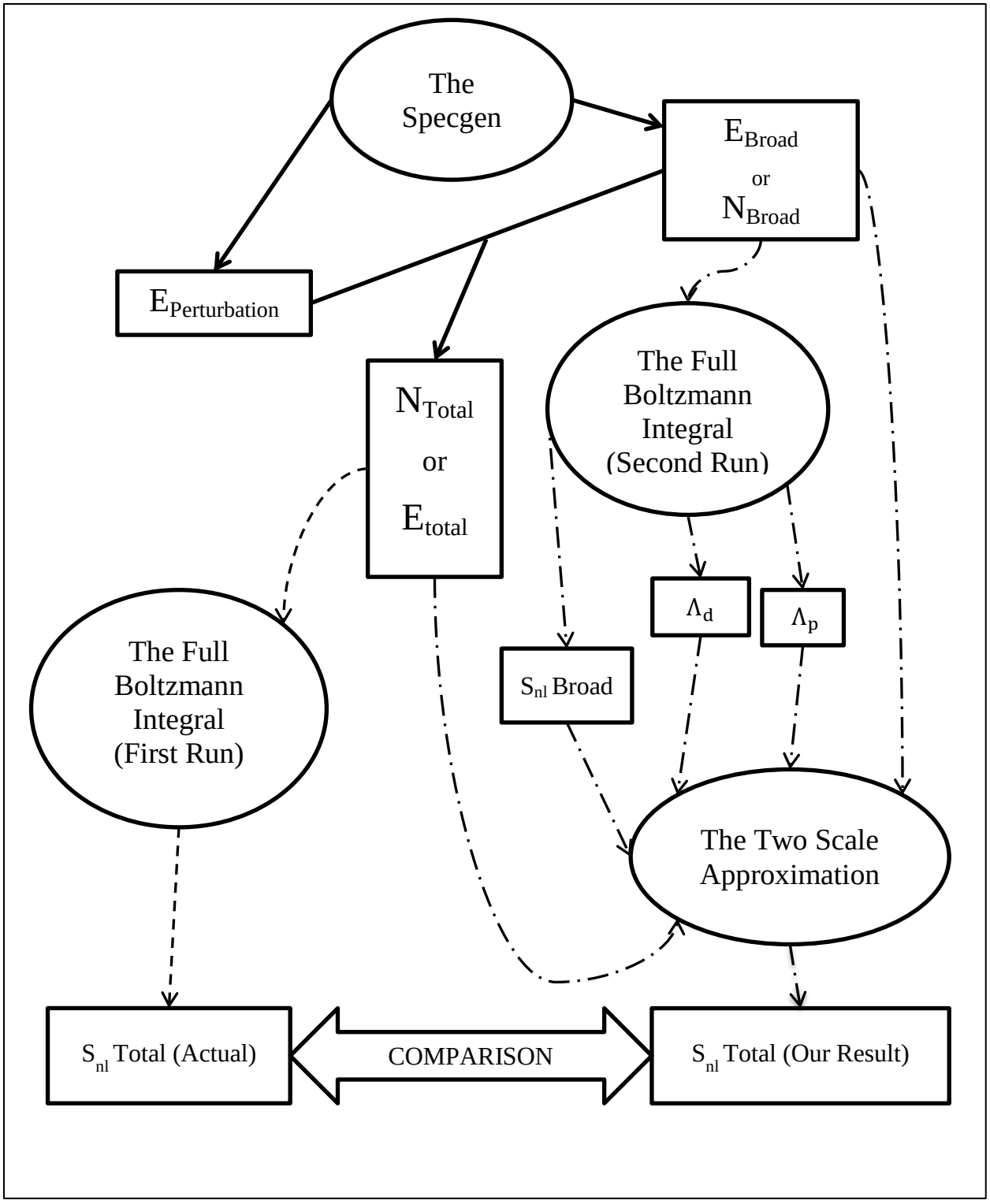

Figure 3–3: The diagram that shows the testing process.

3.2. Modifications

In this section modifications are going to be applied and tested on the TSA program with an intention to make it work more efficiently and much faster. As it was discussed in the first chapter one of the tests is using an energy density spectrum with a small scale perturbation. This will be the primary examination before moving on to the remaining tests.

The intended disturbance is going to be placed on the 23rd ring of the broad scale by using the program the Specgen. The broad scale has a bimodal distribution; with peak frequency is located on the 14th ring or frequency of 0.3 and a frequency multiplier of 1.05. The magnitude of the disturbance is controlled by the input parameter "Apert" in the program for initial testing this value is set to "2". The result of this Specgen execution is displayed on the following figure.

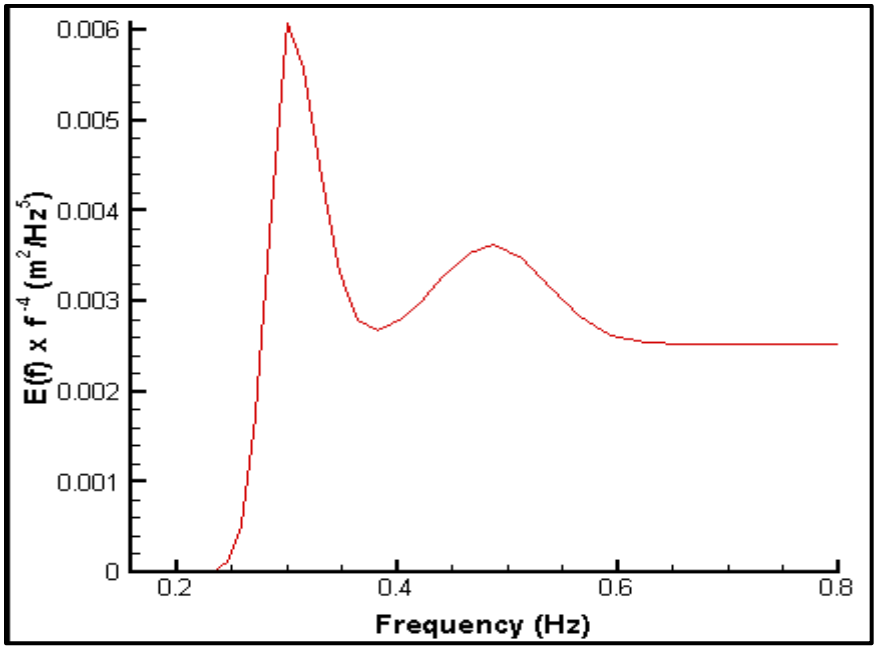

Figure 3–4: Generated input spectra (compensated) with the "Apert" value of 2.

3.2.1. Changing the Domain & Resolution of the Local Scale

The initial TSA local scale had 11 frequencies and 17 angle bands. Alterations here will attempt to reduce the number of these bands and vary the resolution of the local scale since the directly affect the execution time of the model. The input spectrum displayed in the figure 3-4 is going to be used for the first case.

3.2.1.1 Changing the Domain

Changing the domain of the local scale affects the operational speed significantly. For example, reduction in the number of the angle bands from 17 to 15 and the frequency bands from 11 to 9 would make an escalation in the speed of a factor of;

$$\frac{17}{15}\ x\ \frac{11}{9} \sim 1.4$$

For this purpose, first the number of angle bands is going to be decreased until the shape of the final spectrum retains to an acceptable level. After that, the quantity of the frequency bands will be decreased with the same purpose. 1D and 2D comparisons are going to be displayed. For 1D comparisons solid lines are representing the FBI, long dashed lines are the broad scale, dot-dot dashed lines are the DIA and finally dotted dashed lines the TSA.

Figure 3-5 shows the ideal result obtained by using 17 by 11 local scale for the first input.

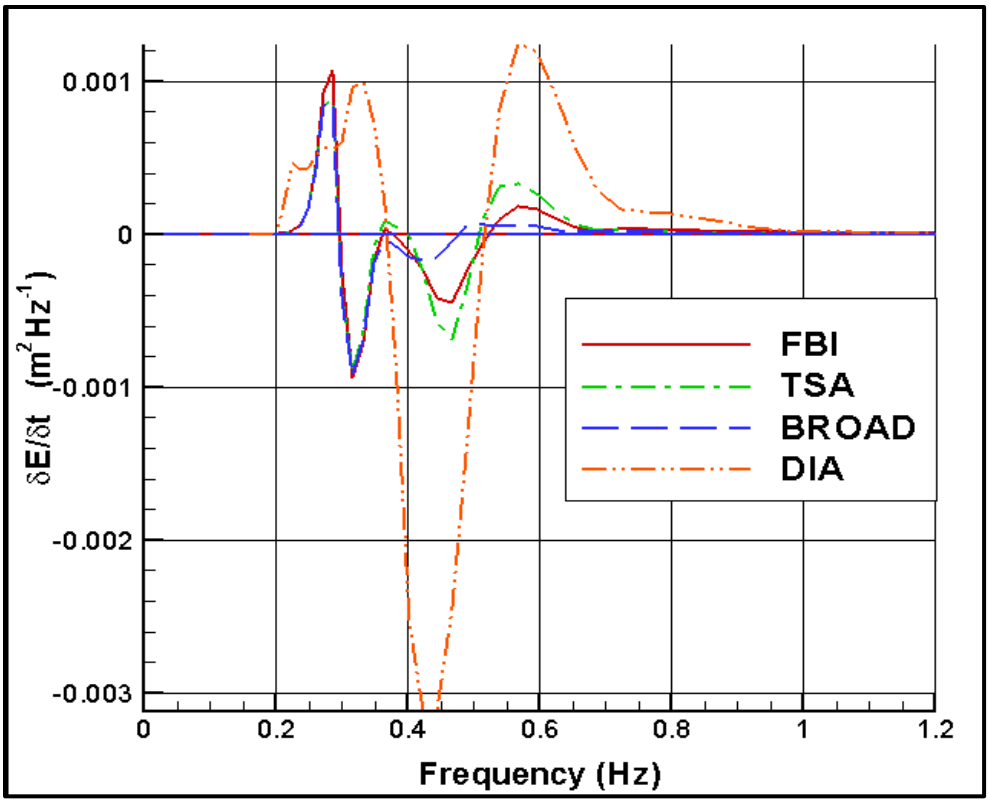

Figure 3–5: The initial TSA plot for the primary examination case.

As it can be seen from the Figure 3-6, we started decreasing the angle bands by reducing it to 11. The plot almost looks alike with the initial results, so we decreased to 7 angle bands. The plot still does not show any significant variation from the initial results. However when it is reduced to 5 angle bands it starts to show minor deformations and deviates from its original shape, yet it still has a great resemblance to the ideal one so it might be acceptable for wave modeling. On the other hand, despite keeping its original form, the plot with 3 angle bands became less acceptable after displaying the amplitudes lower on the lobes than they should be which means there are energy transfers occurring between the 30th and 50th degrees of the grid subset. From this outcome, it can be concluded that decreasing the number of frequency bands slowly changes the

accuracy of the reduced-domain method. The choice of a specific limit would depend on subsequent operational testing.

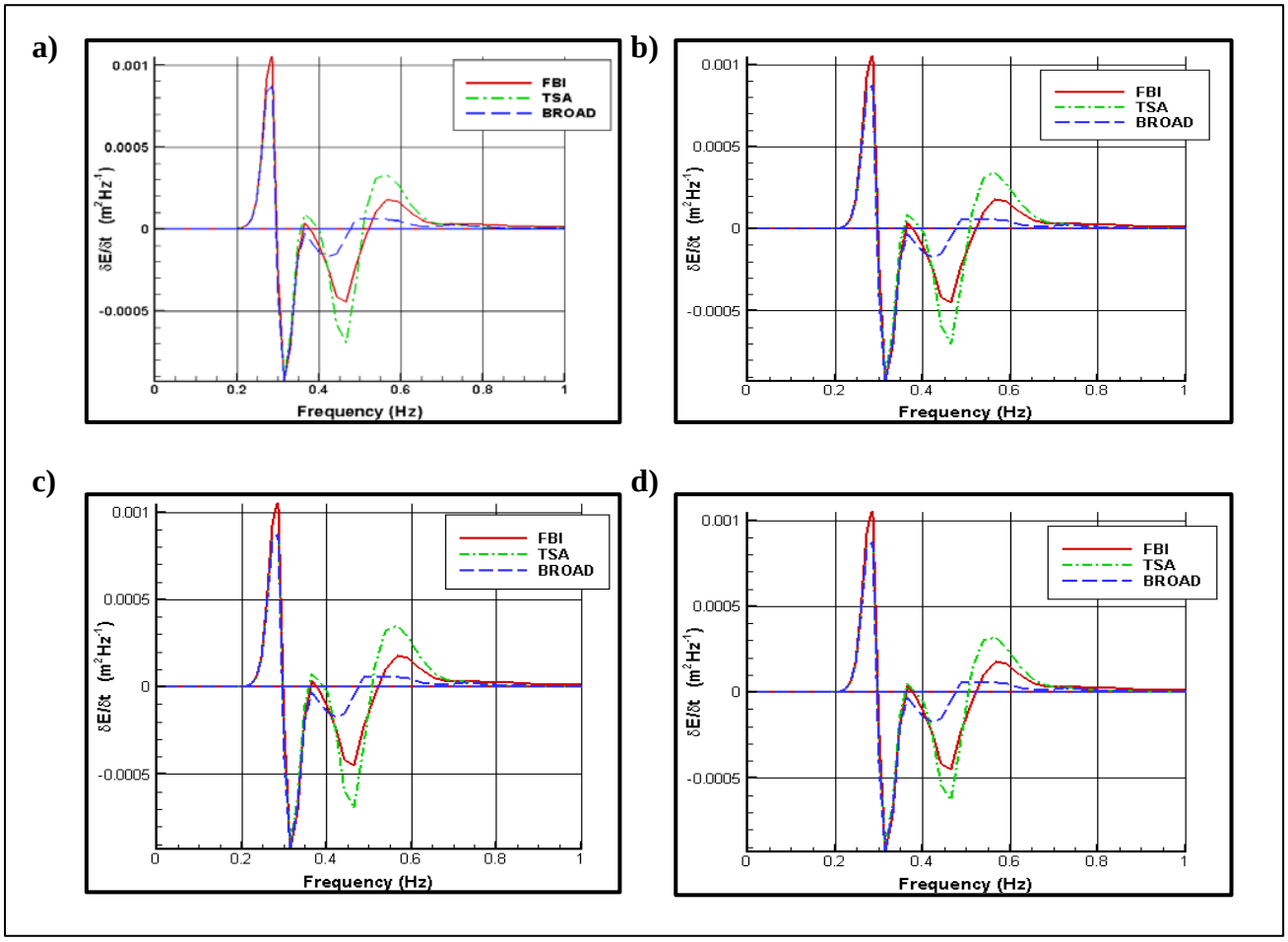

Figure 3–6: The comparisons with 11 frequency bands and a) 11 Angle Bands b) 7 Angle Bands c) 5 Angle Bands d) 3 Angle Bands.

Figure 3-7 includes 3 pair of plots using 8, 5 and 4 frequency bands. The plots with 7 angle bands are on the left side and the plots with 5 angle bands are on the right side. First pair looks successful, as well as the second pair which has lay outs with 5 frequency bands. However

decreasing the frequency grids down to number of 4 ends up with lower magnitudes around the positive and negative lobes which means there are flux transfers happening between 4^{th} and 5^{th} rings of frequency.

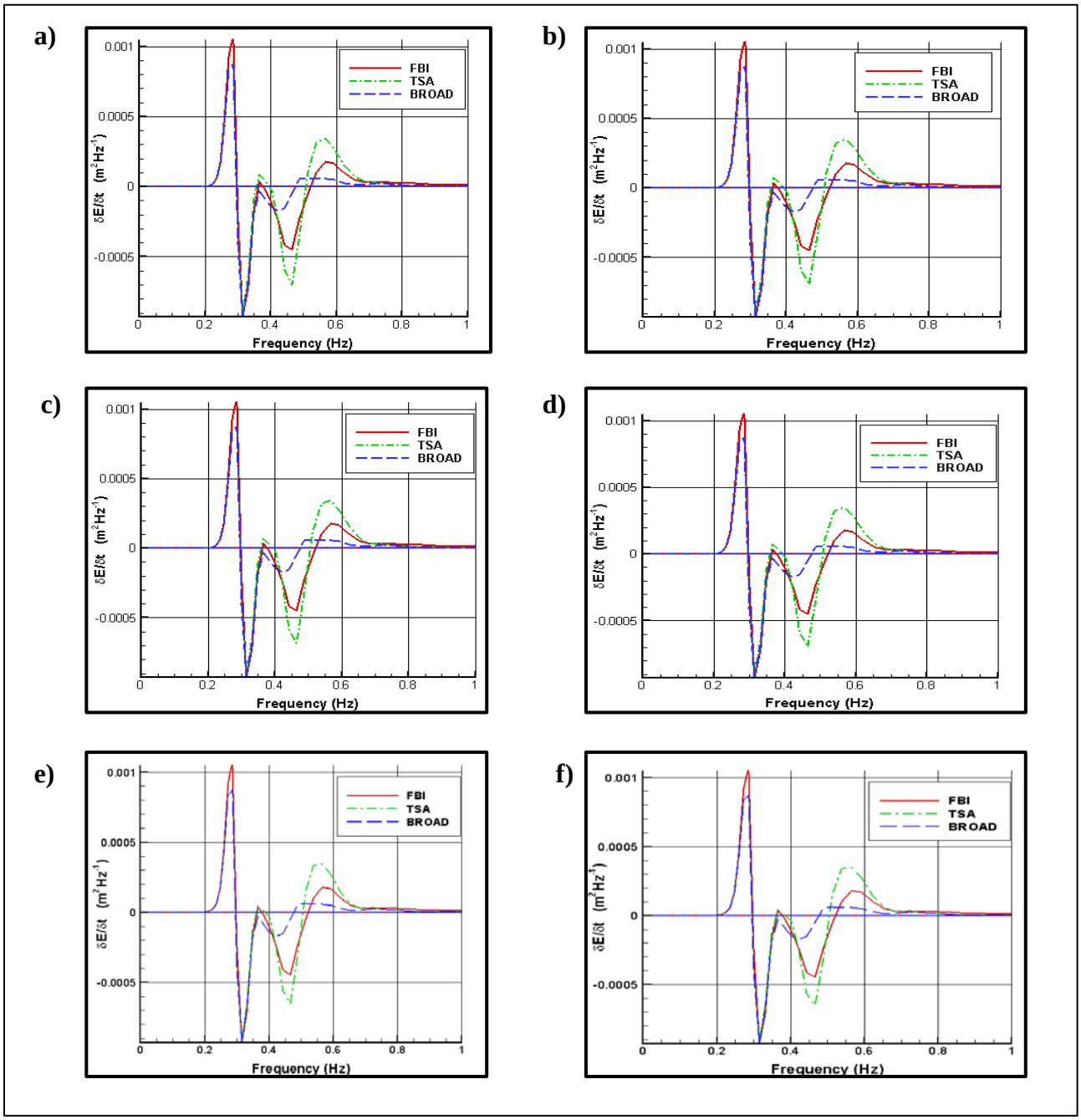

Figure 3–7: The pair of layouts with a) 8 freq. – 7 angle bins b) 8 freq. – 5 angle bins c) 5 freq. – 7 angle bins d) 5 freq. – 5 angle bins e) 4 freq. – 7 angle bins f) 4 freq. – 5 angle bins.

The 5 by 5 size of the local scale seems to work quite reasonably for now, yet for this uncomplicated case the deformations appear to be insignificant, so there needs to be more tests done before reaching a conclusion.

Figure 3-8 includes a 2D comparison to see differences between outcomes of the two methods. For the first test there is not much difference in the shape despite the modification in the TSA method so it confirms with our finding. The TSA domain on this figure uses the 5 by 5(angle bands and frequency bands) local scale.

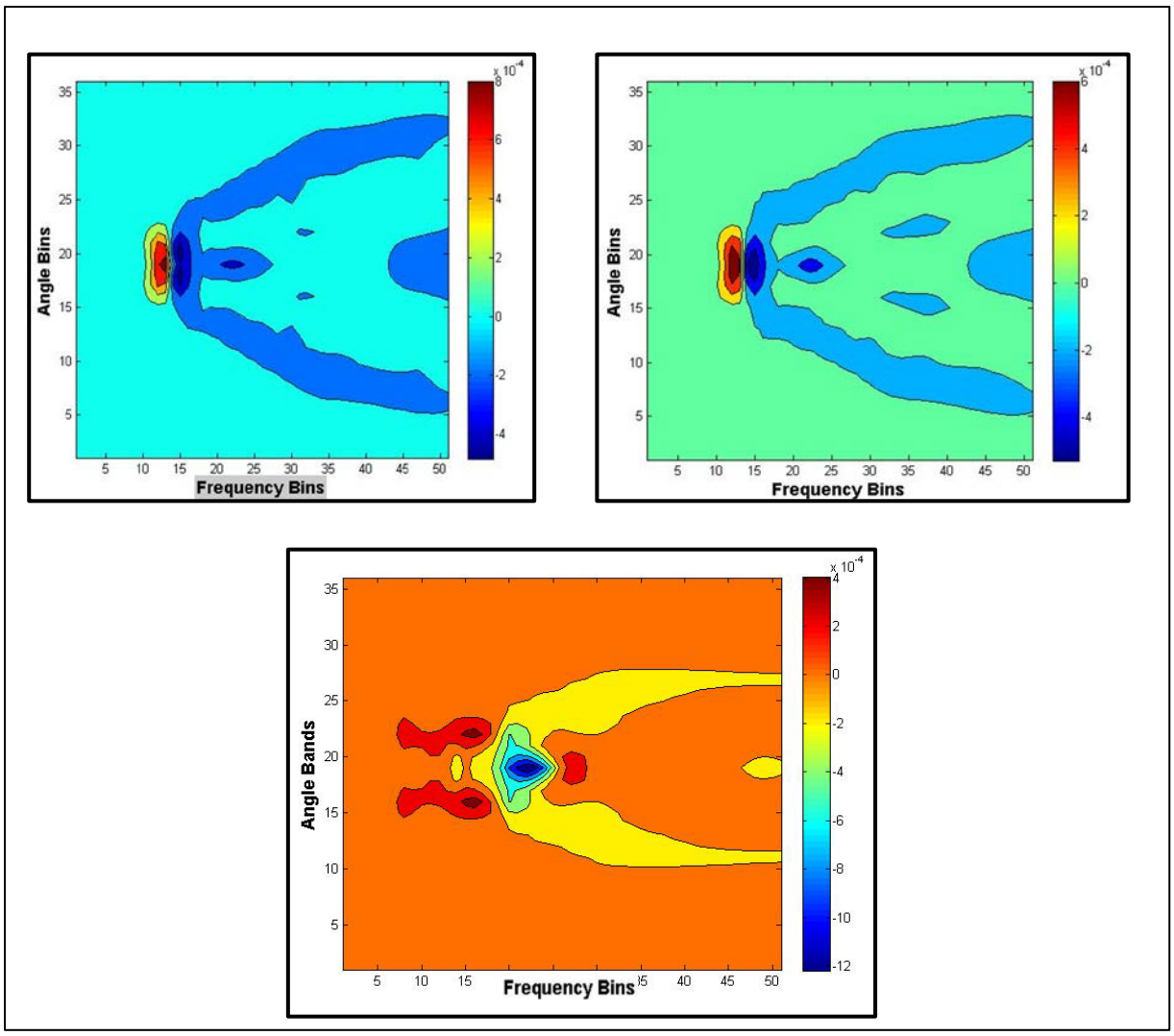

Figure 3–8: A 2D comparison between the FBI (left), the TSA (right) and the DIA (bottom) for the first case.

3.2.1.2 Changing the Resolution

Reducing the resolution implies that using 2 or more bands at a time instead of 1 ring at a time while executing the local-scale integration. For instance, an adjustment which contains using 2

frequency or angle bands in the local scale instead of one band would influence the execution time by a factor of 2.

In the first test 2 frequency bands resolution was used for an initial 17 by 11 local scale and ended up with the following plot;

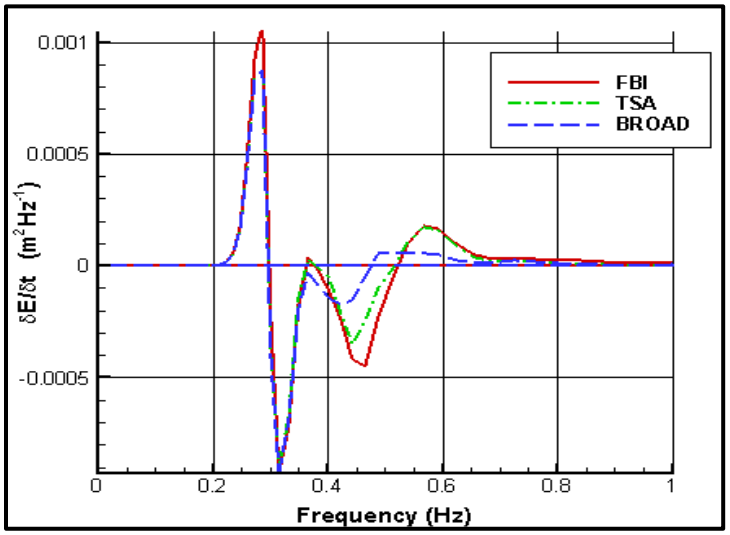

Figure 3–9: The TSA with decreased frequency resolution.

A quick comparison between the figure 3-9 and our initial result easily signifies some divergence between those two. The positive and negative lobes seem to be located correctly however the amplitudes are not represented as accurately as the fully-resolved solution. This deviation led to the decision to not pursue additional reductions in resolution within the scope of this thesis.

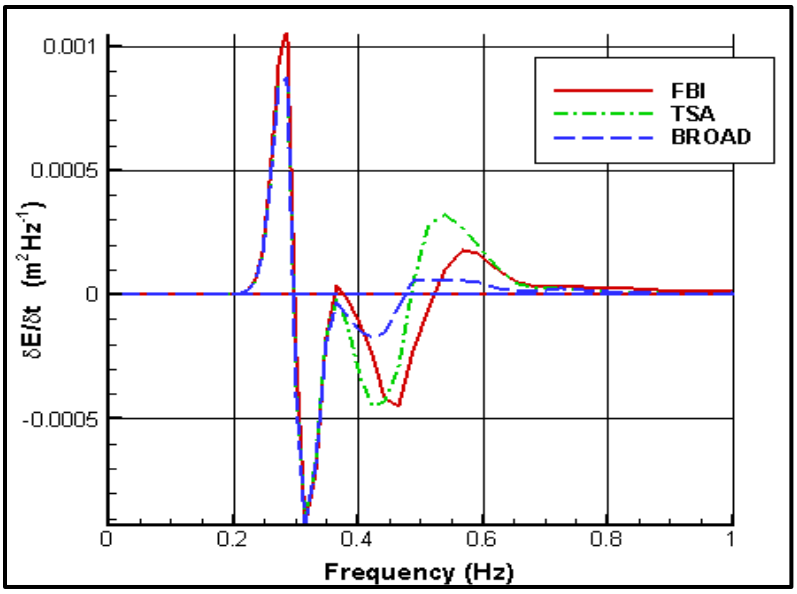

Figure 3–10: The TSA with decreased angular resolution.

Changing the resolution for angle bands produced even large deviations from the fully-resolved solution then altering the resolution for frequency bands. In addition to the deformations in the magnitude, spectral shape also shifted to lower frequencies. Since the purpose of this work which is sustaining the accuracy of the approximation while speeding up the initial TSA, this approach to increase the run speed was not pursued further here.

3.3. Additional Tests to Verify Modifications

The second and third cases examined here will include using different locations and magnitudes for the perturbation. In the second case, the perturbation will be placed on a higher frequency (25^{th} ring) with the Apert value of 4. For the 3^{rd} and the last case the disturbance will be placed on a lower frequency (21^{st} ring) with the Apert value of 4. Third case is the most demanding one among all of the cases. The reason for that is, it has the highest perturbation magnitude since the Apert is a coefficient that is multiplied with the broad scale value it is located on and it makes the 3^{rd} case input a double-peaked spectrum because of the proximate located peaks.

3.3.1. Case 2: 25^{th} Ring – Apert = 4

The input spectra for the second case can be seen on the figure 3-11. The amplitude of the perturbation became larger and its location shifted towards a higher frequency.

Figure 3-12 shows the plot including the results from the FBI, the DIA, the broad scale and the initial TSA run for the second case. The TSA seems to work better when the perturbation is located on a higher frequency. Even the gap between the TSA and the FBI results in the front face of the spectrum got smaller. The reason for this could be when the actual peak and the perturbation gets closer they start to interact with each other. The level of interaction depends on their spreading. As their spreading expands further, they tend to interact more. As a result, it becomes a complex case for the TSA.

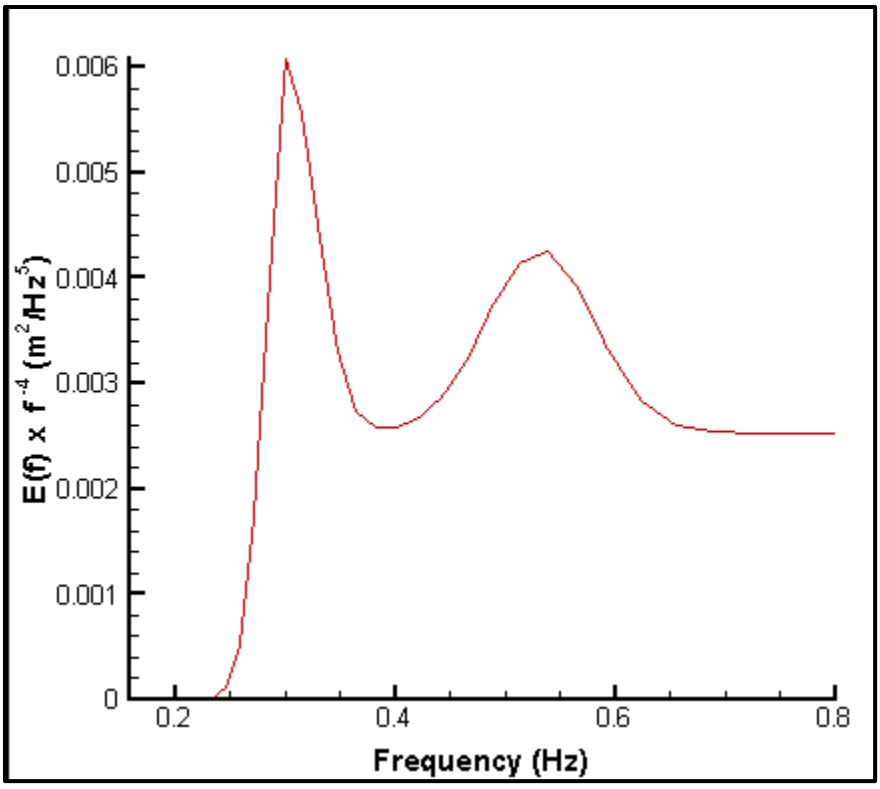

Figure 3–11: Generated input spectra (compensated) with the “Apert” value of 4.

On the other hand, as the peak and the disturbance are located on further rings or they have a lower spreading value there are going to be less complexity for the TSA and the result will be much similar to the FBI.

The tests are going to start with decreasing the number of angle bins and followed by the reducing the number of frequency bins once again.

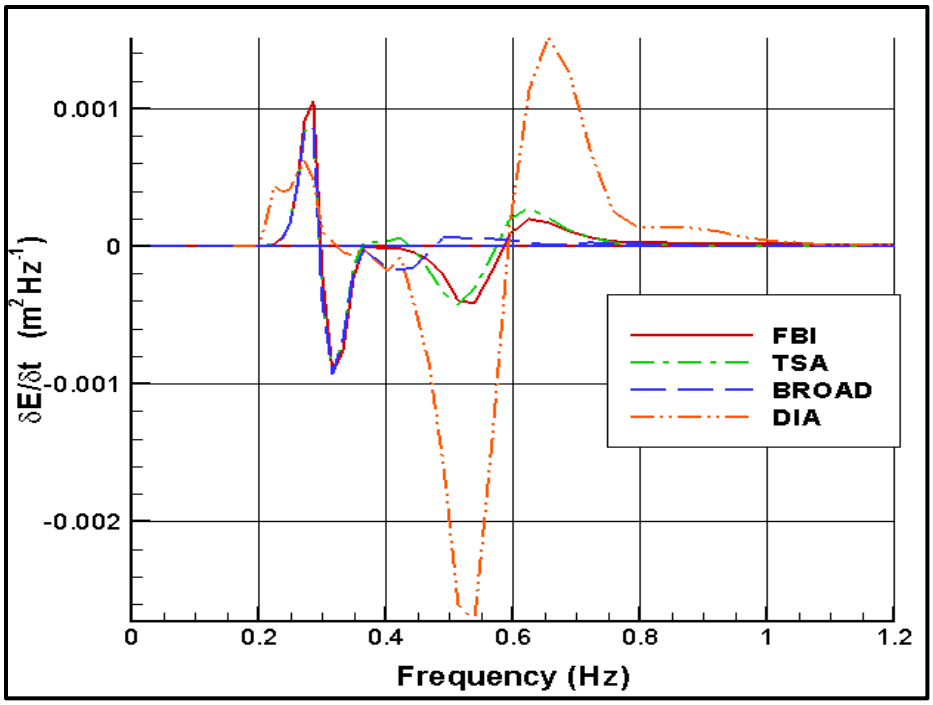

Figure 3–12: The initial TSA result for this case.

On the figure 3-13 there are 4 plots drawn with using 9, 7, 5 and 3 angle bands and 11 frequency grids for the TSA local scale. As similar to the first case, the TSA run with 9 and 7 angle bands work precisely; there are almost no differences between those and the ideal result in the figure 3-12 apart from minor magnitude deviations. The result with 3 angle bands is less acceptable expectedly due to the increased difference between the ideal results. For 5 angle bands, the shape is preserved; however the magnitude difference is slightly higher compared to the 9 and 7 angle bands.

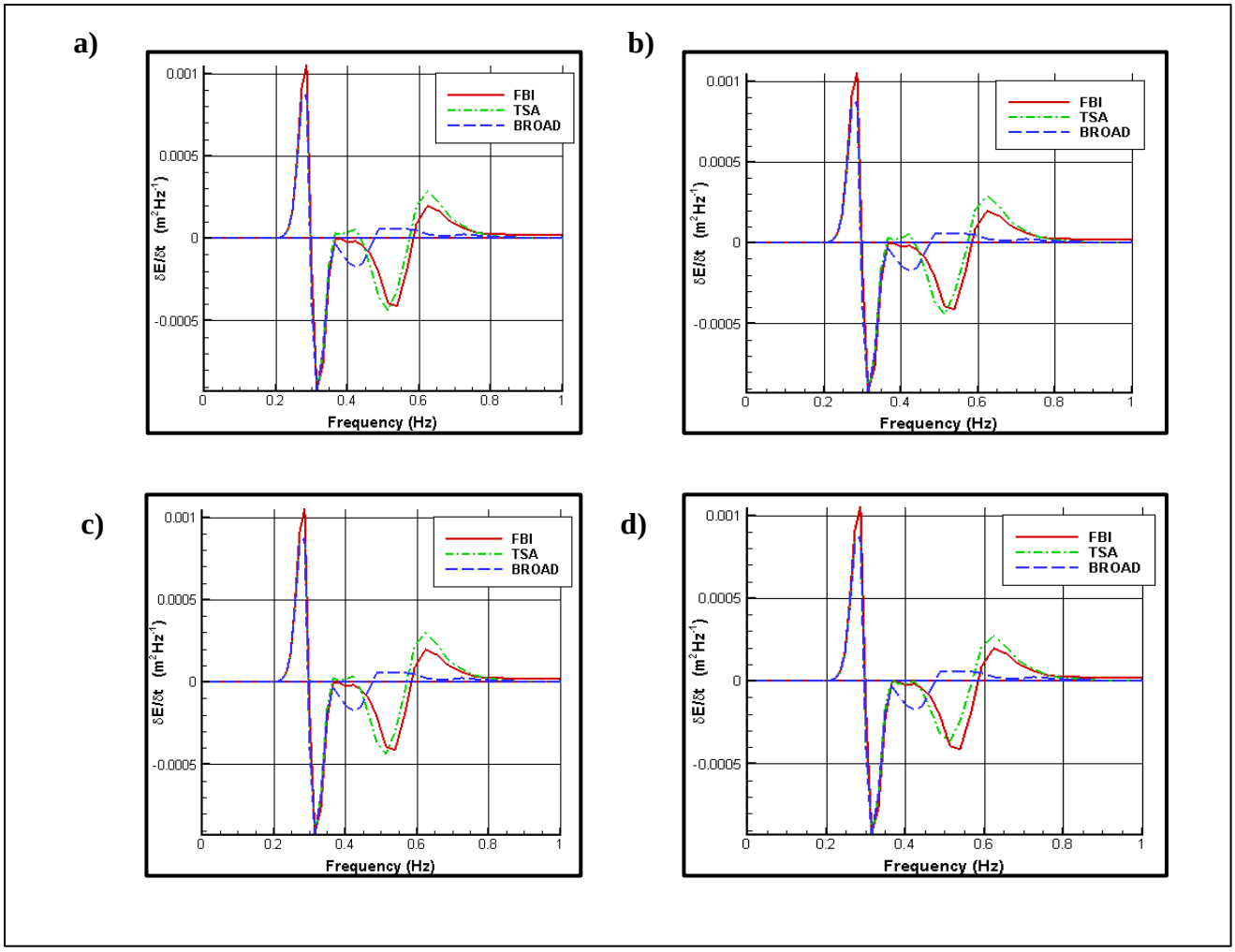

Figure 3–13: The comparisons for the second case with 11 frequency bands and a) 9 Angle Bands b) 7 Angle Bands c) 5 Angle Bands d) 3 Angle Bands.

On figure 3-14, the frequency is decreasing with the values of 8, 5 and 4 and there are plots with 5 and 7 angle bands. These plots confirm that using 4 frequency bands in the TSA local scale reduces the accuracy. In other respects, 8 and 5 frequency bands work quite well. There is some difference after the negative lobe with 5 angle bands and this is for a simpler case than the first one, so using 5 angle bands may not be sufficient for some calculations

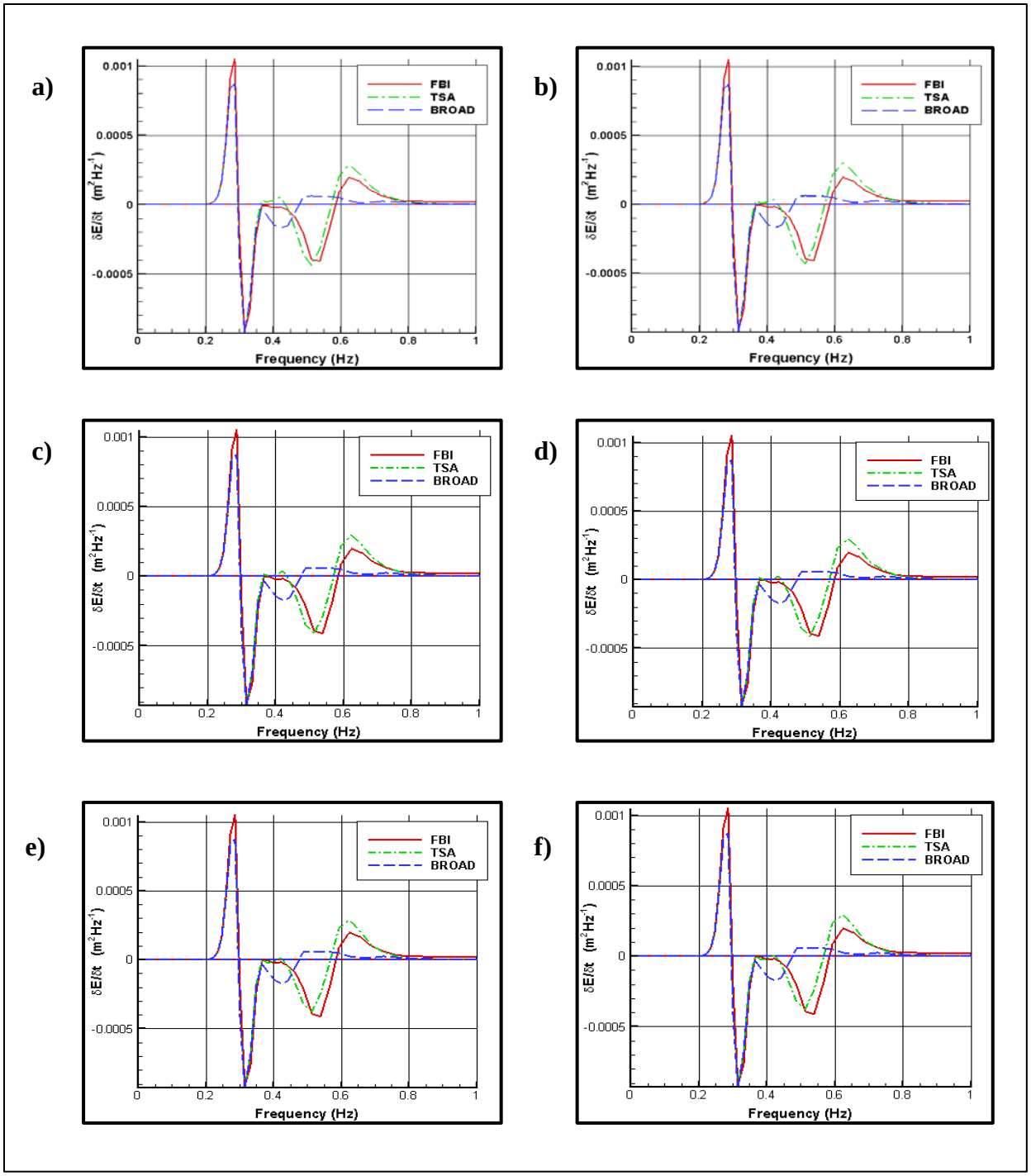

Figure 3–14: The pair of layouts with a) 8 freq. – 7 angle bins b) 8 freq. – 5 angle bins c) 5 freq. – 7 angle bins d) 5 freq. – 5 angle bins e) 4 freq. – 7 angle bins f) 4 freq. – 5 angle bins.

The following figure shows the 2 dimensional comparison between the non-linear transfers calculated using the FBI and the TSA with 5 by 7 local scale. Results for the TSA looks very reasonable, especially considering the performance of the most widely used method, the DIA.

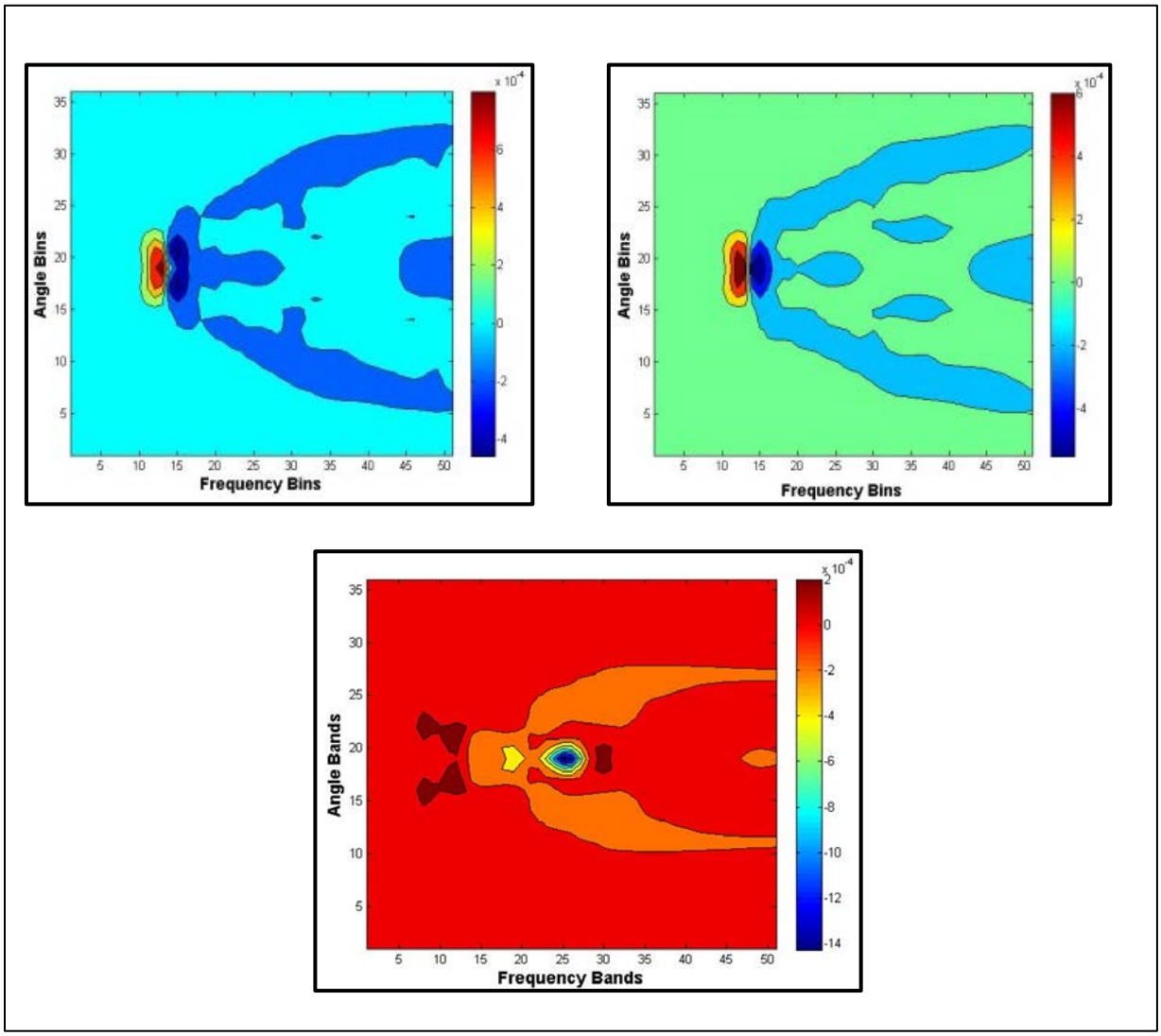

Figure 3–15: A 2D comparison between the FBI (left), the TSA (right) and the DIA (bottom) for the second case. The TSA here has a 5 by 5 local scale.

This work suggests that the optimal grid subset to work with will be a 5 by 7 domain; however the 5 by 5 domain performs almost as well. There is still one last case to run and despite this is the last one it is going to be the most critical case for the TSA with the close positioned perturbation and the actual peak.

3.3.2. Case 3: 21st Ring – Apert = 4

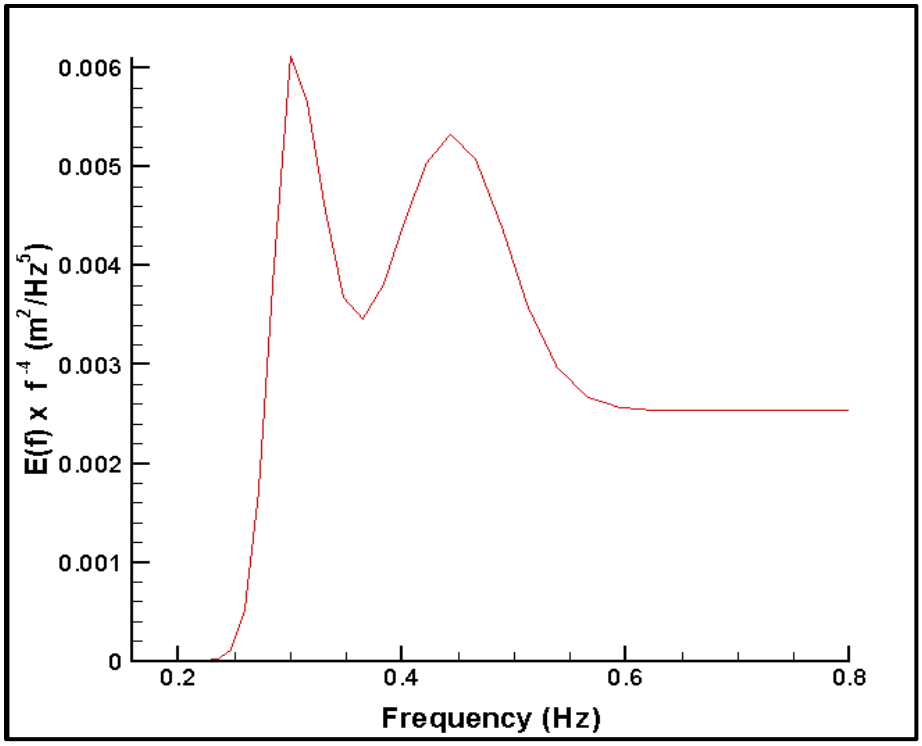

Figure 3–16: Generated input spectra (compensated) with the perturbation located on a closer ring to the peak.

The last generated input spectra is on the figure 3-16. As it can be seen, the perturbation is located really close to the actual peak. Additionally, despite the Apert value remained the same,

the amplitude of the perturbation is larger due to the fact that Apert is a coefficient that is multiplied with the broad scale value it is located on.

From this figure we see that there is one shortcoming of the initial TSA stands out. Since it is still an approximation, it does not work too well for a double-peak case with the peaks in close proximity.

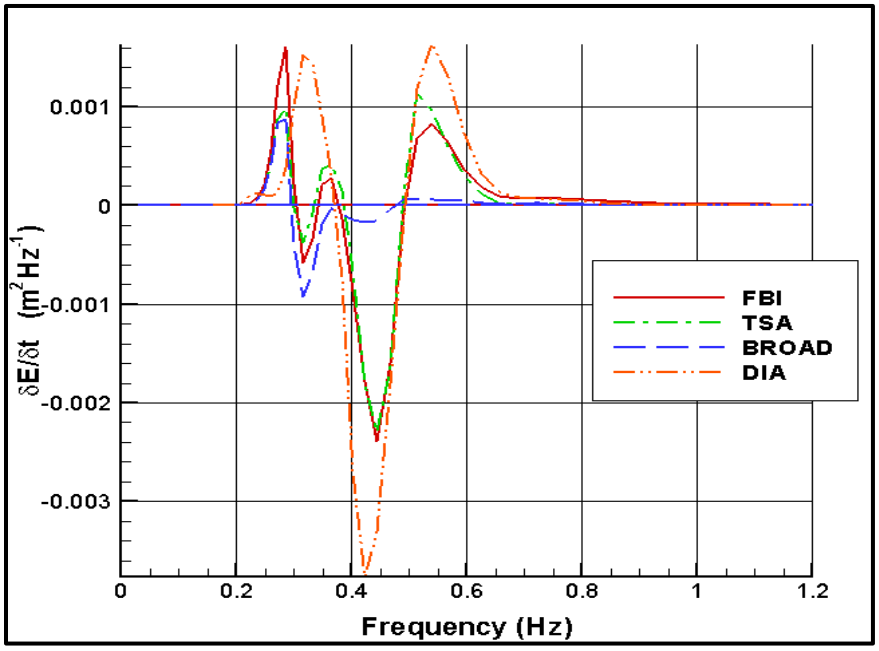

Figure 3–17: The initial TSA result for this case.

For this last and the most difficult case, there are going to be only 6 plots with 7 and 9 angle bands with the frequencies of 5, 6 and 7. The reason for this is to verify the result achieved from the previous two cases that the TSA performs precisely on a local scale of 5 frequency and 7 angle bands. Then we can move on to the next test.

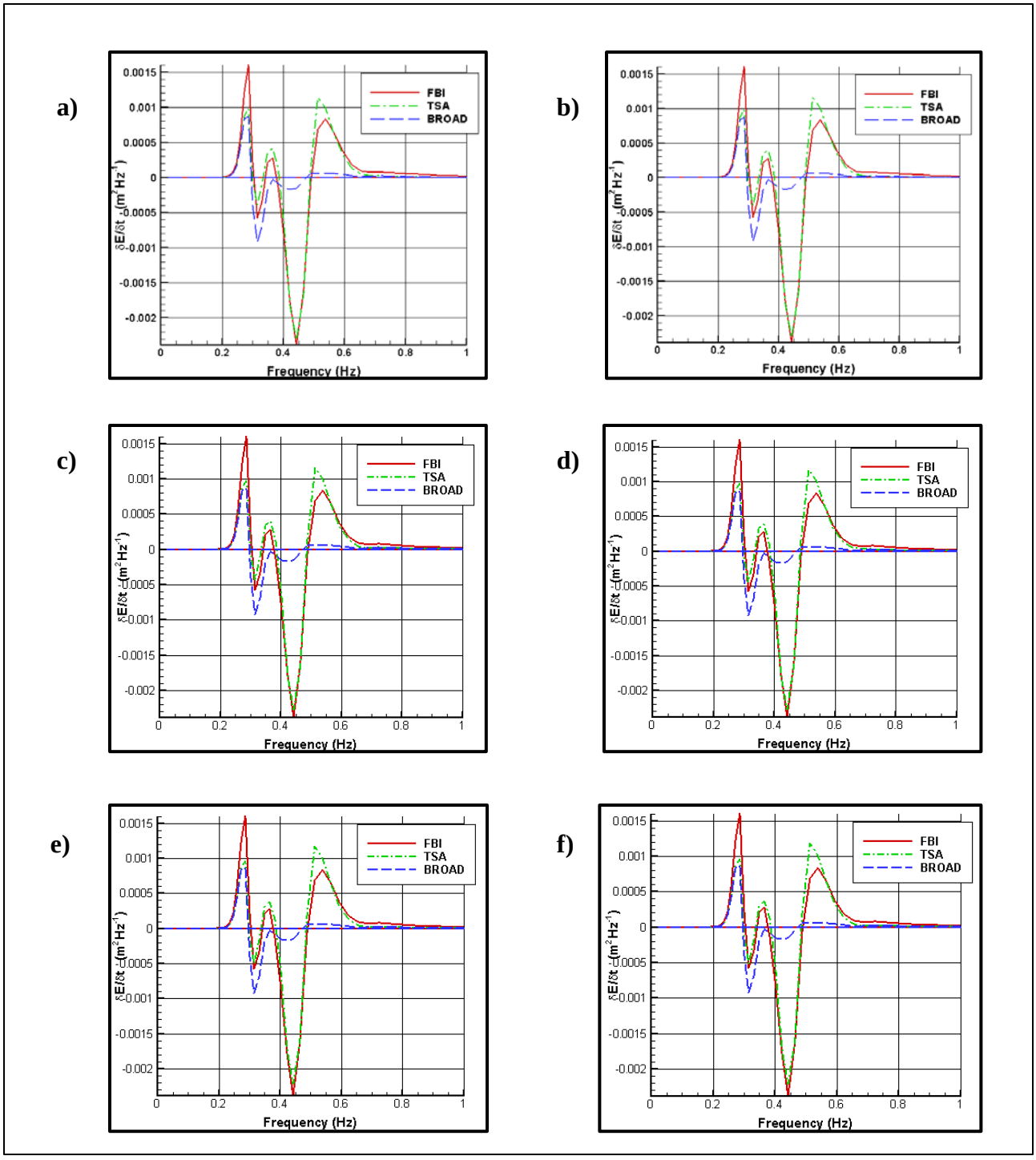

Figure 3–18: The pair of layouts with a) 7 freq. – 9 angle bins b) 7 freq. – 7 angle bins c) 6 freq. – 9 angle bins d) 6 freq. – 7 angle bins e) 5 freq. – 9 angle bins f) 5 freq. – 7 angle bins.

These results can be seen on the figure 3-19. Despite being the final and the most challenging case, the TSA works really well on maintaining the shape for all of the cases. The deformation in the shape only happened during the testing the change in resolution, other than that the modified TSA results always maintained their shape.

In all of the cases the TSA provides a substantially better approximation to the FBI than the DIA which is used in current wave models. The 2D comparison for the third case can be seen from the figure 3-18 and it will help us to understand the success of the improved TSA. The differences in the shape became more obvious for this case but there are two aspects that shouldn't be forgotten here; first of all, this is an approximation method and results cannot be exactly the same, they can be as close as possible. Secondly, the third case is an extreme input spectra, it was only used in the tests to push the limits for the TSA.

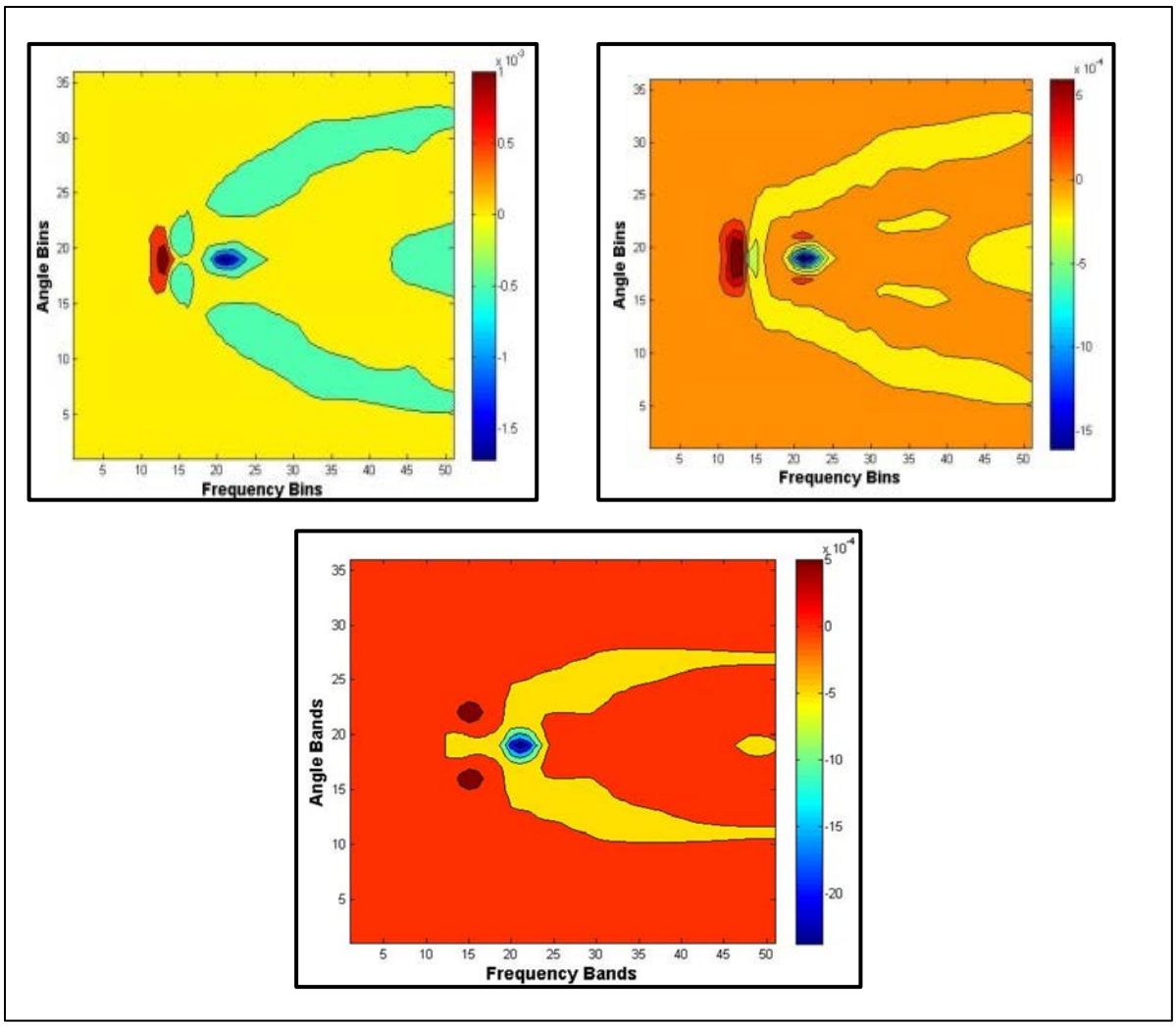

Figure 3–19: The final 2D comparison between the FBI (left), the TSA (right) and the DIA (bottom) for the third case. The TSA here has a 5 by 7 local scale.

From our results and from the aforementioned aspects, it is possible to say using 5 frequency bands instead of 11 and 7 angle bands instead of 17 for local scale is the most ideal choice. However, using 5 by 5 sub grid also did not display much change and might be equally applicable.

The relaxation of the input spectra is desired to be the next test. That is basically investigating the distribution of the perturbation energy to higher and lower frequencies. Those transfer tendencies can also be observed from the plots that we obtained during the tests using the TSA or the FBI methods. As the perturbation gets closer to the peak or the magnitude of it rises, the amplitude of the negative lobe for the S_{nl} also gets bigger. It is because the input spectra try to stabilize it as quickly as possible and when the disturbance is higher the transfers become higher.

3.4. Relaxation of the input spectra

The FBI used in this thesis work is a time-stepping model. It allows user to choose the total duration and time steps. In the figure 3-20 the FBI run over 50 seconds. 1 second time steps are used but only 10 second increments are displayed on this figure. As it can be seen from the figure, the initial spectrum is trying to return a natural state. Because of this, it is trying to get rid of the perturbation energy by distributing it to higher frequencies.

This situation can also be observed on the TSA and the DIA runs, and will be included in future work. What is expected to see is that since the TSA results are very similar to the actual answer we are going to receive a similar relaxation plot. On the other hand, the DIA makes over or under prediction in a lot of frequencies. This will eventually lead to instabilities as the DIA run over more time steps. This is one of the reasons that the DIA needs limitation factors or coefficients in order to run smoothly without failing. Since it is less stable, it also needs smaller time steps to work properly.

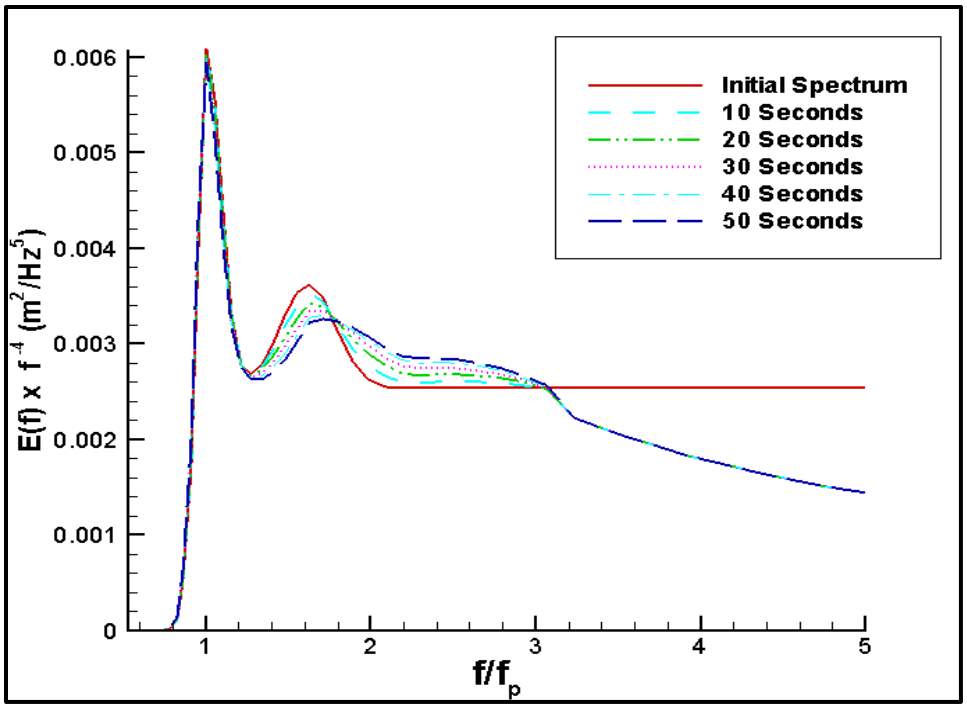

Figure 3–20: The FBI run over 50 seconds with 1 second time steps.

3.5. The effect of modifications on the speed

All the tests completed in this paper implied that the number of the frequency and the angle bands of the local scale can be dropped down to 5 by 7 ideally. Resolution on the other hand cannot be changed. So the total influence of the modifications on the speed is going to be;

$$\frac{17}{7}\ x\ \frac{11}{5} \sim 5.5$$

Initially the TSA was working 13.5 times slower than the DIA. With the impact of the modifications, the final form of the TSA can operate only 13.5/5.5=2.5 times slower than the DIA.

On the other hand using 5 by 5 local scale is also a feasible option. So its influence would be;

$$\frac{17}{5}\ x\ \frac{11}{5} \sim 7.5$$

With the effect of this choice, the final form of the TSA can operate only 13.5/7.5=1.8 times slower than the DIA. Considering the accuracy and the stability advantages of the TSA, a difference of factor of 2.5 or 1.8 in speed is not an intolerable situation, as a matter of fact it shows the TSA is practical enough to be used in an operational model. The fact that the TSA is a method that is open to further development supports our argument.

Chapter 4: DISCUSSION

The main objective of this work was to demonstrate that the Two Scale Approximation could operate with more stability than, and as fast as, the Discrete Interaction Approximation to calculate non-linear wave wave interactions while maintaining its accuracy.

Calculating quadruplet interactions precisely is very crucial for operational wave models. An accurate and fast method will provide correct spectral shapes which are important for coastal processes, coupled models (atmospheric, wave height, storm surge models), remote sensing and understanding of physics (energy fluxes). An accurate spectral shape provides a snapshot of the ocean surface consisting of random waves with frequency information. Two dimensional energy spectra obtained using an approximation method includes angular information besides frequency data. So by using this spectrum not just the magnitude of the energy transfer is understood but also we have an idea about the direction of the energy fluxes.

Another essential aspect of the approximation methods is operating with high stability. These techniques are applied iteratively in wave models, i.e. they operate on their own output from their previous run as the new input. Thus, there should be an agreement between time steps. For instance, if the model is going to run over a total time period of 100 seconds, it completes this process using certain number of time steps. The size of the time step depends on the consistency of the approximation method. A method with a higher stability can operate on bigger time steps whereas if the stability is not sufficient enough, time steps become smaller.

To conceptualize the effect of the time step, it is possible to consider the bigger time step as 0.5 seconds and the smaller one 0.1 seconds. The total assumed duration was 100 seconds. Thus, in order to complete one entire run, the more stable model has to run 100/0.5= 200 times. On the other hand, the less consistent technique has to run 100/0.1=1000 times. Even if all the remaining factors were equal, there would be a 5 times operating speed difference between these two imaginary models. Also, since these are approximation methods, there are going to be minor discrepancies with the FBI every time step, so increasing the total number of time steps is also going to boost these discrepancies with the exact energy spectrum. It is vital to remember that, this is not only for an overall 100 seconds. Considering the size and duration of an operational ocean forecasting model running on, this difference in speed would result in more dramatic variances. Additionally, a less stable method would provide limited accuracy for the operational wave model.

The significance of the operational speed of an approximation method is more apparent than the first two characteristics of accuracy and stability. Although the calculation power of the computer processors are increasing, wave forecasting and the remaining coastal processes are extremely demanding. Despite the fact that some of the major integrals or variables such as the Full Boltzmann Integral were introduced decades ago, it is still not feasible to make actual calculations. Instead, use of an approximation method remains more practical.

Every approximation method must strike a balance between stability, accuracy and speed. For a method to be considered as successful, at least one of these should be strong. The DIA is widely used because of its speed, despite its other well-known deficiencies. In other respects, The TSA

is a very stable and accurate method and it is almost as fast as the DIA. Thus, it is possible to claim that the TSA could replace the DIA.

Another noteworthy point is that, a new method has to be parameterized in order for to be used in an operational wave model. Since the DIA is being widely used for such a long time, it is very integrated into the ocean models and to other applications. Replacing a method like this with a more accurate approximation will be a cumbersome process, despite the advantages it would provide. So, it is highly essential to emphasize the strength of the TSA as well as proving the advantages of using it to substitute this promising method with the DIA.

Chapter 5: CONCLUSIONS AND RECOMMENDATIONS

The Discrete Interaction Approximation, which was used for many years, contains errors related to a misrepresentation of the Full Boltzmann Integral. The Two Scale Approximation showed t is a promising alternative that can be improved with certain modifications and while obtaining those improvements it could also sustain its accuracy within its spectral shape. However, initially the TSA was 13.5 times slower than the DIA. Considering the number of sequences and time periods an operational wave model needs to run, working 13.5 times slower was a crucial issue.

To develop the DIA and the TSA on the FORTRAN environment was the first and the most critical part of this work since they were used continuously in order to produce results which are used to make comparisons. The FBI code and the spectra generator were preprogrammed but also used broadly during testing the modified TSA.

The results from the DIA runs always exhibited very significant problems. Those include not having the correct shape and not representing the amplitudes properly by making over or under predictions around positive or negative lobes of the actual integral. However as a result of the DIA is being used in operational wave models for more than 20 years, its deficiencies are well known. Certain coefficients or limitation factors are used in specific conditions in order to overcome these deficiencies and use the absolute advantage of the DIA which is its speed. Despite using coefficients are burdensome, it is still the most preferred approach.

The TSA was modified primarily by changing the constant $\cos^{2n}(\theta - \theta_0)$ spreading to variable spreading and defining a new reference spectrum for the broad scale term (Chapter 1). Further possible modifications involved changing its local scale by either altering the limits or the resolution of the domain. Also running the TSA on a continuous basis instead of a discrete one was critical. In all of the tests continuous basis was used and it was successful.

The deformation in the shape only happened during the testing the change in resolution, other than that the modified TSA results always maintained their shape. During the tests there was a gap between the TSA and the FBI results located in the front face of the spectrum. The reason for this could be when the actual peak and the perturbation gets closer they start to interact with each other. The level of interaction depends on their spreading. As their spreading expands further, they tend to interact more. However, this should be further investigated

Changing the resolution did not give the desired outcomes in spite of its potential huge boost in speed. The end product was either shifted or had extreme differences with the original energy spectrum. On the other hand, by different kind of tests, it was shown that decreasing the domain of the local scale, the TSA could perform faster and precisely without affecting its accuracy. This decrease was tested with three cases which had perturbations with two magnitudes and placed on various parts of the broad scale spectrum. It was concluded that using 5 frequency bands and 7 angle bands for the local scale is ideal and resulted with an increase of 5.66 in speed for the TSA. On the other hand using 5 frequency bands and 5 angle bands for the local scale is feasible and can increase the speed by a factor of 7.5. This means that the modified TSA now works only 1.5

times slower than the DIA, which is probably not significant for its application to operational wave models.

Considering that the TSA is still open to further development and boosting up to speed even more a difference of 1.8 is not a major difference. Additionally, the TSA`s stability is higher compared to the DIA and it is going to help the TSA to be able to operate on larger time steps than the DIA could operate on.

REFERENCES

Cardone, V. J., W. J. Pierson, and E. G. Ward. "Hindcasting the Directional Spectra of Hurricane-Generated Waves." *Journal of Petroleum Technologies, Vol. 28*, 1976: 385-394.

Gelci, R., H. Cazalé, and J. Vassal . "Sea state forecasting. The spectral method (In French)." *Bulletin d'information du Comité d'Océanographie et d'Etude des Côtes, Vol.9*, 1957: 416-435.

Hasselmann, Klaus. "On the non-linear energy transfer on a gravity-wave spectrum. Part 1. General Theory." *Journal of Fluid Mechanics. Vol. 12*, 1961: 481-500.

Hasselmann, Susanne, Klaus Hasselmann, J.H. Allender, and T.P. Barnett. "Computations and Parametrizations of the Nonlinear Energy Transfer in a Gravity-Wave Specturm. Part II: Parameterizations of the Nonlinear Energy Transfer for Application in Wave Models." *Journal of Physical Oceanography* 15 (1985): 1378-1391.

Holthuijsen, Leo H. *Waves in Oceanic and Coastal Waters.* 1st. Cambridge University Press, 2007.

Perrie, Will, Bechara Toulany, Donald T. Resio, Aron Roland, and Jean-Pierre Auclair. "A two-scale approximation for wave–wave interactions in an operational wave model." *Ocean Modelling, Vol.70*, 2013: 38-51.

Phillips, O. M. "The equilibrium range in the spectrum of wind-generated waves." *Journal of Fluid Mechanics. Vol. 4*, 1958: 426-434.

Resio, Donald T., and Charles E. Long. "The Role of Nonlinear Momentum Fluxes on the Evolution of Directional Wind-Wave Spectra." *Journal of Oceanography, Vol. 41*, 2011: 781-801.

Resio, Donald T., and William Perrie. "A Two-Scale Approximation for Efficient Representation of Nonlinear Energy Transfers in a Wind Wave Spectrum. Part I: Theoretical Developement." *Journal of Physical Oceanography, Vol. 38*, 2008: 2801-2816.

Resio, Donald T., and William Perrie. "A Two-Scale Approximation for Efficient Representation of Nonlinear Energy Transfers in a Wind Wave Spectrum. Part II: Application to Observed Spectra." *Journal of Physical Oceanography, Vol. 39*, 2009: 2451-2475.

Tracy, and Resio. ""Theory and calculation of the nonlinear energy transfer between sea waves in deep water"." Wave Information Study Rep. No. 11, U.S. Army Engineer Waterways Experiment Station., Vicksburg, MS., 1978, 54.

WAMDI Group. "The WAM Model- A Third Generation Ocean Wave Prediction." *Journal of Physical Oceanography, Vol. 18*, 1988: 1775-1810.

Webb, D.J. "Non-linear transfers between sea waves." *Deep-Sea Research, Vol. 25,* 1978: 279-298.